REPORT

NEURODEVELOPMENT

Multicluster Pcdh diversity is required for mouse olfactory neural circuit assembly

George Mountoufaris,[1,2]† Weisheng V. Chen,[1,2]*† Yusuke Hirabayashi,[2,3] Sean O'Keeffe,[1,2] Maxime Chevee,[1,2] Chiamaka L. Nwakeze,[1,2] Franck Polleux,[2,3] Tom Maniatis[1,2]‡

The vertebrate clustered protocadherin (Pcdh) cell surface proteins are encoded by three closely linked gene clusters (*Pcdhα*, *Pcdhβ*, and *Pcdhγ*). Here, we show that all three gene clusters functionally cooperate to provide individual mouse olfactory sensory neurons (OSNs) with the cell surface diversity required for their assembly into distinct glomeruli in the olfactory bulb. Although deletion of individual *Pcdh* clusters had subtle phenotypic consequences, the loss of all three clusters (tricluster deletion) led to a severe axonal arborization defect and loss of self-avoidance. By contrast, when endogenous Pcdh diversity is overridden by the expression of a single–tricluster gene repertoire (α and β and γ), OSN axons fail to converge to form glomeruli, likely owing to contact-mediated repulsion between axons expressing identical combinations of Pcdh isoforms.

The vertebrate clustered protocadherin *Pcdhα*, *Pcdhβ*, and *Pcdhγ* genes (Fig. 1) generate a high level of cell surface diversity in the nervous system by a mechanism of stochastic promoter choice (*1*, *2*) and assembly of α, β, and γ protein monomers into combinatorial cis homo- or heterodimers that engage in homophilic interactions at the cell surface (*3*–*5*). Functional studies in mice revealed that the *Pcdhγ* gene cluster is required for dendritic self-avoidance in retinal starburst amacrine cells (*6*). However, it remains unclear why a self-avoidance phenotype was not observed in most other neuronal cell types examined in either *Pcdhγ* (*7*–*11*) or *Pcdhα* (*12*) single cluster deletion mutant mice.

Here, we address the functional significance of the multicluster organization of *Pcdh* genes, focusing on the wiring of mouse olfactory sensory neurons (OSNs). Individual OSNs monoallelically express a single olfactory receptor (OR) (referred to as "like-OSNs") (*13*, *14*) and project their axons to the olfactory bulb (OB) to form glomeruli (*15*). RNA-sequencing analysis of bulk (fig. S1A), as well as individual, OSNs (Fig. 1) (*16*, *17*) revealed that individual mature OSNs (mOSNs) stochastically express distinct combinations of alternate Pcdh isoforms from all three gene clusters. However, unlike the Purkinje cells (*18*) in which both alternate and C-type isoforms are expressed, the C-type Pcdh isoforms were detected in only a small fraction of mOSNs (Fig. 1 and tables S1 and S2). Moreover, both alternate and C-type isoforms were expressed in immature OSNs (fig. S1A). Thus, the C-type Pcdh isoforms are selectively down-regulated during OSN maturation.

To determine the function of the entire *Pcdh* gene cluster in OSN wiring, we generated mice in which the 1 million base pairs of DNA spanning all three gene clusters were deleted (*Pcdhα*, *Pcdhβ*, *Pcdhγ*–tricluster deletion) (figs. S2 and S3). Because of the neonatal lethality of the tricluster-deletion pups, our analyses were carried out at postnatal day 0 (Fig. 2). A severe protoglomerular (glomeruli of newborns) phenotype was observed in the *Pcdh* tricluster deletion mice (Fig. 2, A to C). Although, most like-*Pcdh*–null OSN axons converged to their approximately normal coordinates in the bulb, they failed to form normal-appearing protoglomeruli (fig. S4A). To visualize the effect of the tricluster deletion on individual OSNs, they were labeled by using an in utero electroporation method adapted for the olfactory epithelium (fig. S5A), and their morphology was examined as they project to the bulb. As shown in Fig. 2G, individual OSN axons in the tricluster deletion neonates did not display the normal "cup"-shaped axonal arbors observed in control mice. Rather, mutant axonal arbors appeared heavily clumped and distorted, indicative of the loss of self-avoidance, resulting in the formation of abnormal protoglomeruli (Fig. 2, G and H, and fig. S5, B to E).

We next generated mice in which each of the *Pcdh* gene clusters was deleted (fig. S2). By contrast to the severe phenotype observed in the tricluster-deletion mice, deletion of the *Pcdhα* gene cluster led to the appearance of somewhat less compact protoglomeruli, consistent with a previous report of *Pcdhα* hypomorphic mice (*19*) (Fig. 2D). In addition, no major discernible defect in protoglomeruli formation was found when either the *Pcdhβ* or *Pcdhγ* gene cluster was deleted, as compared with the mice having a tricluster deletion (Fig. 2, A to F, and see material and methods). Taken together, these deletion studies indicate that, in the complete absence of multicluster Pcdhs, "sister" axonal arbors from individual OSNs fail to recognize self and thus display the clumped phenotype. However, in the absence of the *Pcdhα* or *Pcdhβ* or *Pcdhγ* gene cluster alone, the remaining two gene clusters provide individual OSNs with sufficient cell surface

[1]Department of Biochemistry and Molecular Biophysics, Columbia University, New York, NY 10032, USA. [2]Mortimer B. Zuckerman Mind Brain Behavior Institute, Columbia University, New York, NY 10032, USA. [3]Department of Neuroscience, Kavli Institute for Brain Science, Columbia University, New York, NY 10032, USA.
*Present address: Kallyope, Inc., New York, NY 10016, USA.
†These authors contributed equally to this work.
‡Corresponding author. Email: tm2472@cumc.columbia.edu

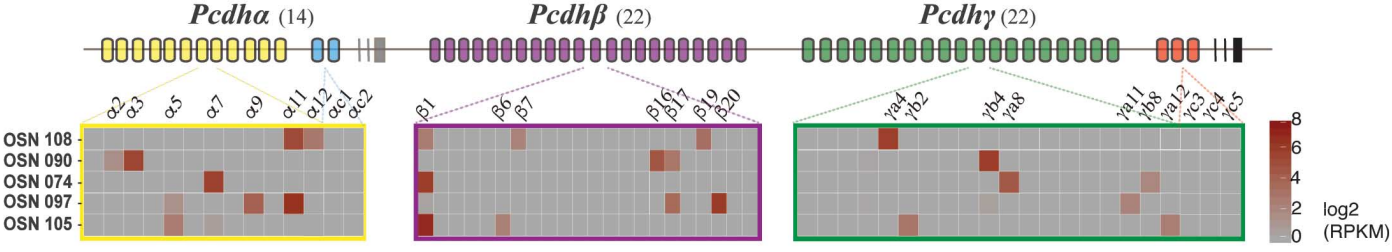

Fig. 1. Distinct combinations of Pcdhα, -β, and -γ isoforms are stochastically expressed in individual OSNs. Pcdh isoforms are divided into two categories, the alternate (indicated by the yellow, purple, and green ovals) and the C-type (indicated by the blue and red ovals). Single-cell, stochastic expression of Pcdhα and -β and -γ isoforms in five different mOSNs. Note the absence of detectable *Pcdhα* or -γ c-type expression in these cells (see tables S1 and S2). The presence of individual Pcdh isoform mRNA is indicated by red-colored boxes, and the levels are indicated by the color gradient [$\log_2$ reads per kilobase of transcript per million mapped reads (RPKM)].

diversity required for self-recognition and the formation of protoglomeruli.

To further explore the role of multicluster Pcdh diversity in olfactory circuit assembly, we established an OSN-cell–autonomous gain-of-function approach. Specifically, we sought to override the endogenous multicluster Pcdh single-cell diversity by expressing high levels of either one of two distinct sets of three Pcdh isoforms (α and β and γ) (uni-Pcdhs) (UNI1 and UNI3) (fig. S6, A and B, and fig. S12) exclusively in mOSNs. We found that the ectopic expression of the uni-Pcdh cassette did not affect OR choice (fig. S14), OR expression (fig. S13A), or OSN maturation (fig. S13B). However, a striking phenotype was observed in whole mounts and coronal sections of the olfactory bulbs of the uni-identity mice (both in UNI1 and UNI3): the absence of glomeruli in the olfactory bulb (Fig. 3 and fig. S6, B and D). Thus, the normal axonal interactions required for the postnatal assembly of glomeruli do not occur when the endogenous Pcdh diversity of individual OSNs was replaced with a single-tricluster Pcdh identity.

We next asked whether OSNs expressing the uni-Pcdh cassettes project to their normal sites of glomerulus formation in the OB. Specifically, we examined three different OSN populations that form glomeruli at distinct locations in the bulb by directly crossing the uni-identity mice to OR-specific reporter lines. We found that, in adult animals, OSN axons expressing the same OR, as well as the same set of Pcdhα and -β and

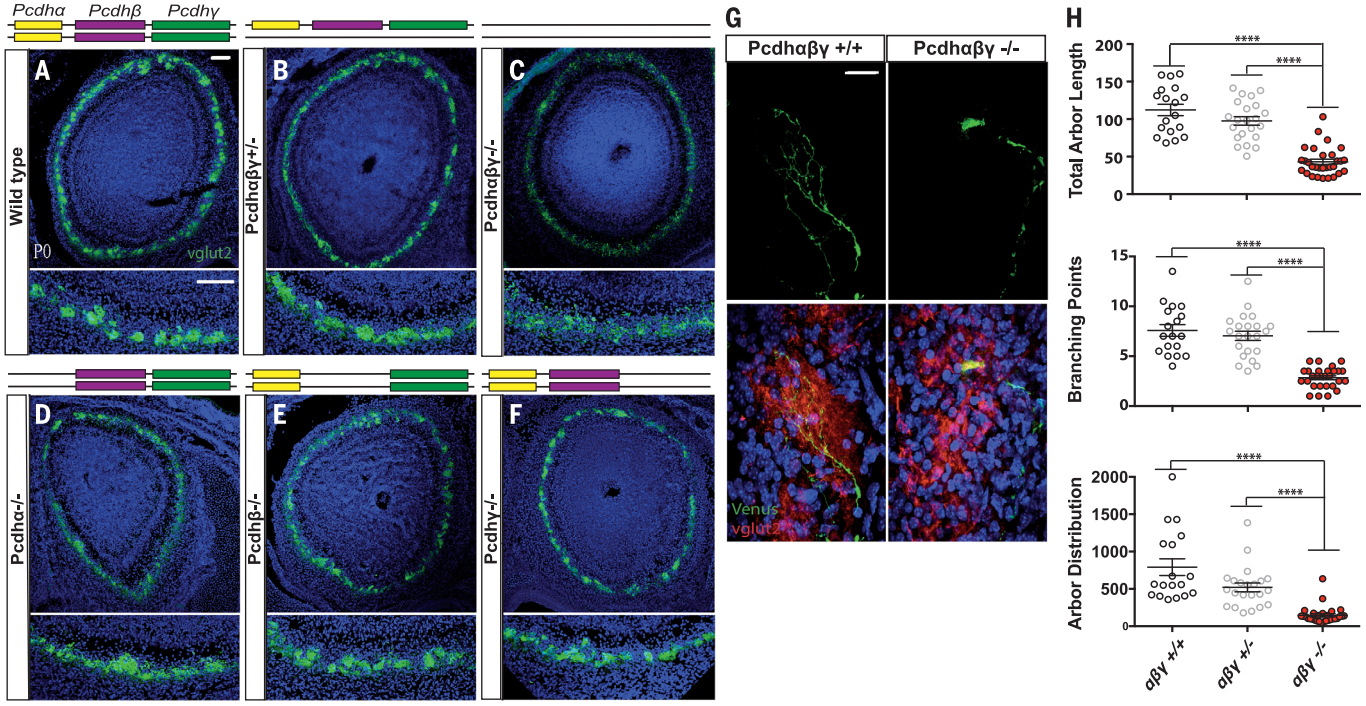

Fig. 2. Multiple *Pcdh* gene clusters are required for normal OSN axonal arborization and the formation of normal protoglomeruli. (**A**) Immunohistochemistry (IHC) against vesicular glutamate transporter 2 (*vglut2*) gene expression in coronal sections through the anterior OB of (A) wild-type, (**B**) *Pcdh*αβγ$^{+/-}$, (**C**) *Pcdh*αβγ$^{-/-}$, (**D**) *Pcdh*α$^{-/-}$, (**E**) *Pcdh*β$^{-/-}$, and (**F**) *Pcdh*γ$^{-/-}$ pups. Coronal section of the entire anterior bulb (top) and a zoomed-in area (bottom) through the OB. The three *Pcdh* gene clusters are indicated by the colored boxes. (**G**) IHC against Venus and vglut2 in utero electroporated OSNs from control and *Pcdh*αβγ$^{-/-}$ mice. (**H**) Quantification of the total length, the number of branch points, and the two-dimensional distribution of OSN arbors in *Pcdh*αβγ$^{+/+}$ (n = 18), *Pcdh*αβγ$^{+/-}$ (n = 22), and *Pcdh*αβγ$^{-/-}$ mice (n = 32) ($n \geq 6$ pups per genotype; Kruskal-Wallis test, $P < 0.0001$). Error bars represent SEM. DAPI, 4′,6-diamidino-2-phenylindole (blue). All Pcdh-tricluster mutant mice bear also the bacterial artificial chromosome Tg (see fig. S2). Scale bars: (A) to (F), 100 μm; and (G), 20 μm.

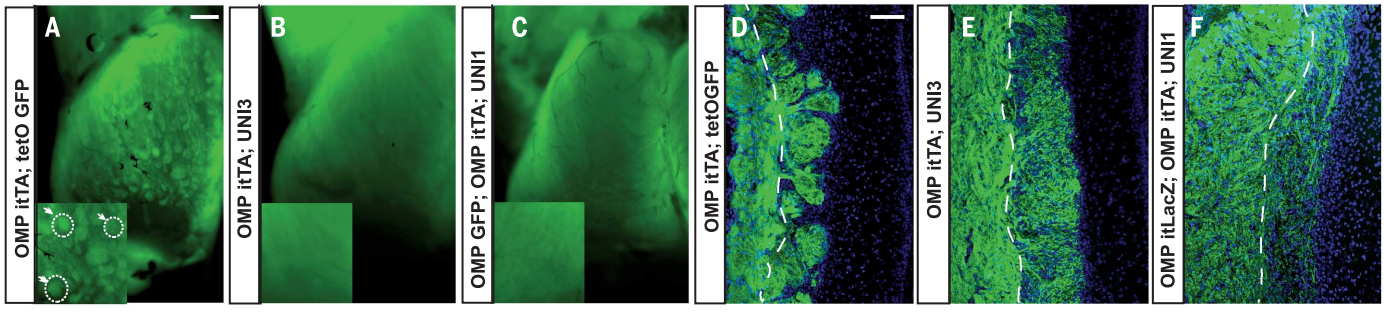

Fig. 3. Uni-identity OSN axons fail to form glomeruli. Whole-mount fluorescence microscopy images of the dorsal OB in (**A**) control and (**B** and **C**) uni-identity 4- to 5-week-old mice (mouse strains on figure). Arrows and circles highlight glomeruli in whole-mount zoom images. IHC against GFP, TagT, and β-galactosidase (β-Gal) in a coronal section through the OB in (**D**) control and (**E** and **F**) uni-identity 4- to 5-week-old mice. Dashed line designates the separation of the nerve layer (NL, left side) and the glomerular layer (GL, right side). TagT and β-Gal are pseudo-colored green; DAPI, blue. Scale bars: (A) to (C), 500 μm; (D) to (F), 100 μm.

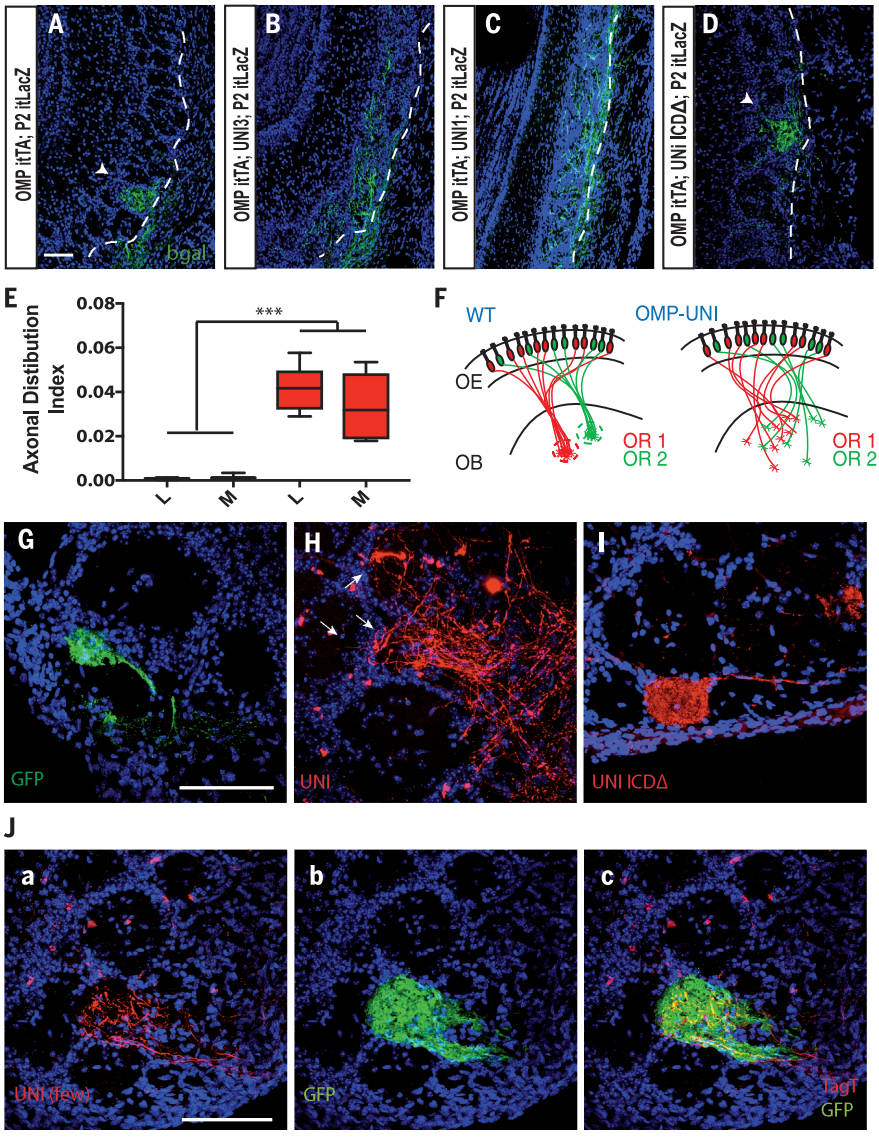

Fig. 4. Uni-identity like-OSN axons fail to converge in the OB. IHC against β-Gal in coronal sections through the OB in (**A**) control, (**B** and **C**) uni-identity, and (**D**) UNI ICDΔ in 4-week-old mice. Arrows depict the P2 medial glomerulus. Dashed line designates the separation of NL (right) and GL (left). β-Gal is pseudo-colored green. (**E**) Quantification of P2 axonal distribution of lateral and medial projections in the OB of 8-week-old control (black, $n = 9$ bulbs), and uni-identity mice (red, $n = 6$ bulbs). (Mann-Whitney test, medial $P = 0.0002$, lateral $P = 0.0004$). (**F**) Normally, like-OSN axons (OR1, red, and OR2, green) converge into stereotypically positioned glomeruli within the OB (left). OE, olfactory epithelium. In uni-identity mice, OSN axons that share the same single dominant Pcdh uni-identity project diffusely to their expected positions in the OB (right). (**G**) Expression of GFP or (**H**) UNI3, or (**I**) UNI ICDΔ cassette exclusively in MOR28 OSNs. Arrows depict the aberrant projection of MOR28-UNI axons in the bulb. [**J** (**a** to **c**)] The few MOR28-UNI axons localize with wild-type MOR28 OSNs labeled with GFP. Animals were 4 to 5 weeks old. DAPI, blue. Scale bar, 100 μm.

-γ isoforms (uni-Pcdhs), projected diffusely to their approximately normal stereotypic locations in the bulb but failed to organize into distinct glomeruli (Fig. 4, A to C; fig. S7; and fig. S8, B and C). Moreover, this lack of axonal convergence (Fig. 4, E and F) persisted throughout development, suggesting that uni-Pcdh–expressing axons have reached their "final" destinations in the OB (fig. S8A). Considering the absence of normal glomeruli in uni-identity mice, it was surprising to find that they were not anosmic (fig. S9, C and D). However, the uni-identity mice did display defects in odor discrimination (fig. S9, A and B). We note that the uni-identity OSN wiring phenotype required intact full-length Pcdh proteins, as apparently normal glomeruli were observed when the uni-Pcdh cassette was replaced with truncated Pcdh mutant isoforms in which either the extracellular domains (UNI ECDΔ) [required for homophilic interactions (*3*)] (fig. S11) or the intracellular domains (UNI ICDΔ) [thought to mediate intracellular signaling (*20*)] were deleted (Fig. 4D and fig. S10, A to C).

To address the selectivity and the underlying mechanism by which the uni-identity phenotype emerges, we examined the effect of overriding endogenous Pcdh diversity exclusively in like-OSNs, i.e., those expressing the same OR (e.g., the MOR28 receptor). In this case, if the presence of uni-Pcdhs mediates repulsion between individual OSN axons, the formation of MOR28-specific glomeruli should be prevented, without interfering with the assembly of all other glomeruli. We generated mice in which the majority of MOR28 OSNs expressed uni-Pcdh's, whereas other types of OSNs expressed only the endogenous Pcdh's. As predicted, MOR28-UNI axons failed to converge to form a glomerulus but instead spread into the territories of adjacent wild-type glomeruli (Fig. 4H). By comparison, control MOR28 OSN axons formed normal-appearing glomeruli (Fig. 4, G and I). These data substantiate the hypothesis that, as individual MOR28 OSN axons ("like-axons") expressing the same uni-Pcdhs converge to a common site in the bulb, they inappropriately recognize each other as being axons of the same neuron. As a consequence, Pcdh-mediated contact-dependent repulsion likely occurs between these like-axons and thus prevents them from converging to form a glomerulus.

We next examined animals expressing the uni-Pcdhs in only a limited number of MOR28 OSNs. We hypothesized that the presence of large numbers of wild-type MOR28 axons, each with its own Pcdh identity, would substantially "dilute" the uni-identity axons and, in essence, rescue or diminish the convergence phenotype (i.e., by minimizing the likelihood that MOR28-UNI axons will encounter each other during axonal convergence and glomerulus assembly) (fig. S15B). Indeed, as shown in Fig. 4J, the small number of MOR28-UNI axons project to the "right" location in the bulb [detected by the green fluorescent protein–positive (GFP+) wild-type axons] and form a close-to-normal glomerulus. These results show that the severity of the convergence defect of MOR28-UNI axons increases as larger numbers of interacting axons sharing the same Pcdh identity converge on the site of glomerulus formation (fig. S15C). More important, this observation is consistent with the notion that individual OSN axons displaying the same set of Pcdhα, -β, and -γ isoforms repel each other because of inappropriate Pcdh-dependent self-avoidance.

Here, we demonstrate that the mouse *Pcdhα*, *Pcdhβ*, and *Pcdhγ* gene clusters functionally complement each other to provide individual OSNs with sufficient levels of Pcdh cell surface diversity required for OSN wiring. This observation likely explains the lack of widespread neuronal wiring defects in mice bearing single–*Pcdh* gene–cluster deletions (*7*–*11*). Our studies also highlight the surprisingly similar logic by which the mouse clustered Pcdh and *Drosophila* Down syndrome cell adhesion molecule (Dscam) proteins function in analogous structures in the olfactory system. In both cases, loss of function leads to "clumping" of OSN axon termini during

glomeruli formation (*21*), whereas loss of single-cell diversity results in the absence of normal glomerular structures (*22*).

In addition, our observations reveal different modes of *Pcdh* gene regulation that depend on the identity of the expressing neuron: the stochastic expression of variable exons in the case of mOSNs and a deterministic expression of *Pcdhac2* in serotonergic neurons (*23*). This differential *Pcdh* gene expression likely reflects the unique requirement for normal wiring of the two neuronal cell types. In the case of olfactory neurons, multicluster diversity in *Pcdh* expression is required for convergence of like-axons to form glomeruli. By contrast, serotonergic neurons express the same C-type isoform, which mediates homotypic axonal repulsion, ensuring even distribution of their axon termini in the brain (*23*). Thus, the same multiclustered *Pcdh* gene family functions in glomeruli formation by olfactory neurons and tiling by serotonergic neurons, providing a remarkable example of functional diversification of a gene family accomplished simply by the evolution of distinct transcriptional programs.

REFERENCES AND NOTES

1. B. Tasic *et al*., *Mol. Cell* **10**, 21–33 (2002).
2. X. Wang, H. Su, A. Bradley, *Genes Dev.* **16**, 1890–1905 (2002).
3. R. Rubinstein *et al*., *Cell* **163**, 629–642 (2015).
4. D. Schreiner, J. A. Weiner, *Proc. Natl. Acad. Sci. U.S.A.* **107**, 14893–14898 (2010).
5. C. A. Thu *et al*., *Cell* **158**, 1045–1059 (2014).
6. J. L. Lefebvre, D. Kostadinov, W. V. Chen, T. Maniatis, J. R. Sanes, *Nature* **488**, 517–521 (2012).
7. W. V. Chen *et al*., *Neuron* **75**, 402–409 (2012).
8. A. M. Garrett, D. Schreiner, M. A. Lobas, J. A. Weiner, *Neuron* **74**, 269–276 (2012).
9. J. Ledderose, S. Dieter, M. K. Schwarz, *Sci. Rep.* **3**, 1514 (2013).
10. J. L. Lefebvre, Y. Zhang, M. Meister, X. Wang, J. R. Sanes, *Development* **135**, 4141–4151 (2008).
11. X. Wang *et al*., *Neuron* **36**, 843–854 (2002).
12. S. Hasegawa *et al*., *Mol. Cell. Neurosci.* **38**, 66–79 (2008).
13. L. Buck, R. Axel, *Cell* **65**, 175–187 (1991).
14. A. Chess, I. Simon, H. Cedar, R. Axel, *Cell* **78**, 823–834 (1994).
15. P. Mombaerts *et al*., *Cell* **87**, 675–686 (1996).
16. L. R. Saraiva *et al*., *Sci. Rep.* **5**, 18178 (2015).
17. L. Tan, Q. Li, X. S. Xie, *Mol. Syst. Biol.* **11**, 844 (2015).
18. S. Esumi *et al*., *Nat. Genet.* **37**, 171–176 (2005).
19. S. Hasegawa *et al*., *Front. Mol. Neurosci.* **5**, 97 (2012).
20. W. V. Chen, T. Maniatis, *Development* **140**, 3297–3302 (2013).
21. T. Hummel *et al*., *Neuron* **37**, 221–231 (2003).
22. D. Hattori *et al*., *Nature* **449**, 223–227 (2007).
23. W. V. Chen *et al*., *Science* **356**, 10.1126/science.aal3231 (2017).

ACKNOWLEDGMENTS

We thank R. Axel and S. Lomvardas for generously providing mouse lines and reagents and R. Axel, S. Lomvardas, and C. Zuker for their advice and critical input throughout the course of this project and their critical reading and advice on the manuscript. D. Canzio, P. Kratsios, W. Grueber, and members of the Maniatis laboratory also provided critical reading of the manuscript. We thank G. Barnea for the MOR28 antibody and L. Tan, Q. Li, and X. S. Xie for sharing their single-cell OSN RNA-sequencing data. D. Kato provided assistance with the behavioral assay, and excellent technical and mouse support was provided by A. Struve, M. Mendelsohn, and A. Kirner. This work was supported by NIH grant R01N5088476. The supplement contains additional data.

SUPPLEMENTARY MATERIALS

www.sciencemag.org/content/356/6336/411/suppl/DC1
Materials and Methods
Figs. S1 to S16
Tables S1 and S2
References (*24*–*33*)

11 November 2016; accepted 16 February 2017
10.1126/science.aai8801

Multicluster Pcdh diversity is required for mouse olfactory neural circuit assembly

George Mountoufaris, Weisheng V. Chen, Yusuke Hirabayashi, Sean O'Keeffe, Maxime Chevee, Chiamaka L. Nwakeze, Franck Polleux and Tom Maniatis (April 27, 2017)

Science **356** (6336), 411-414. [doi: 10.1126/science.aai8801]

Editor's Summary

Pattern formation in the brain

Neurons in the developing brain cooperate to build circuits. Mountoufaris *et al.* found that ~50 variable protocadherin genes support a combinatorial identity code that allows millions of olfactory neuron axons to sort into ~2000 glomeruli. Sharing olfactory receptors drives axons to one glomerulus, and protocadherin diversity allows the multiple axons to touch each other as they converge. On the other hand, Chen *et al.* found that a single C-type protocadherin underlies the tiled distribution of serotonergic neurons throughout the central nervous system. These neurons, which share protocadherin identity, enervate broad swaths evenly without touching neighboring neurons.

Science, this issue p. 411, p. 406

Science (print ISSN 0036-8075; online ISSN 1095-9203) is published weekly, except the last week in December, by the American Association for the Advancement of Science, 1200 New York Avenue NW, Washington, DC 20005.

www.sciencemag.org/content/356/6336/411/suppl/DC1

Supplementary Materials for

Multicluster Pcdh diversity is required for mouse olfactory neural circuit assembly

George Mountoufaris,* Weisheng V. Chen,* Yusuke Hirabayashi, Sean O'Keeffe, Maxime Chevee, Chiamaka L. Nwakeze, Franck Polleux, Tom Maniatis†

*These authors contributed equally to this work.

†Corresponding author. Email: tm2472@cumc.columbia.edu

Published 28 April 2017, *Science* **356**, 411 (2017)
DOI: 10.1126/science.aai8801

This PDF file includes

Material and Methods

Published mouse strains

All mice were housed in the Columbia vivarium under standard conditions with a 12 hr light/dark cycle and access to food and water ad libitum and in accordance with the Columbia University IACUC guidelines. Previously published mouse strains used in this study are as follows: OMP-IRES-GFP, OMP-IRES-tTA (*21*); OMP-IRES-tau-LacZ, P2-IRES-tau-lacZ (*13*); MOR28-IRES-Cre, MOR28-IRES-GFP (*24*); M71-IRES-tau-GFP (*25*), Ngn1-GFP (*26*), Pcdhγ::GFP(*10*) and Pcdhγ -/-(*11*).

Generation of UNI, UNI ICD*Δ*, A-Γ ECD*Δ* mice

Each construct bearing the cDNA from full length or truncated Pcdh isoforms was cloned into a pTRE2 plasmid upstream of the WPRE sequence and polyA signal. The plasmid constructs were linearized, purified, and injected in FVB embryos (Columbia Transgenic Core). Pups born from surrogate mothers were positive for the transgenes. The Transgenic founders where crossed with OMP-IRES-tTA mice and the progeny showing high levels of Transgene expression in OSNs were used for analysis. All mice were maintained in a mixed genetic background.

Generation of cluster deletion alleles

Deletions of *Pcdhα*, *Pcdhβ*, and all three Pcdh gene clusters (*Pcdhαβγ*) were generated in a similar fashion to the *Pcdhγ* gene cluster deletion allele (*11*) by chromosome engineering. HPRT-deficient HM-1 ES cells of 129/ola origin were used to engineer these alleles. Briefly, the 5' and 3' ends of the gene cluster(s) to be deleted were sequentially targeted with insertional targeting vectors carrying a partial HPRT minigene, followed by transient Cre expression and HAT selection for HPRT complementation to enrich for the rare long-range deletion events. Drug-resistant ES cell clones were screened with long-range PCR using internal and external primers, and the PCR products sequenced to verify that the desired recombination events had occurred. Primer sequences used for genotyping will be provided upon request. ES cells bearing the deletions were microinjected into C57BL/6J blastocysts to generate chimeras, and the animals were then bred to produce heterozygous and homozygous animals. The BAC transgene was engineered by first removing all neighboring Pcdh genes by recombination, leaving only the four non-Pcdh genes (*Slc25a2*, *Taf7*, *AK150172*, *AK149307*) that span ~60 kb. The engineered BAC construct was microinjected into C57BL/6J embryos to produce transgenic founders, from which independent transgenic lines were established. All mice were maintained in a mixed 129 and C57BL/6J genetic background.

Immunofluorescence

DAPI was used at 1ug/ml, secondary antibodies were Alexa conjugates from Invitrogen. Sections were cut from either fresh-frozen tissue or post fixed 2h 4%PFA on ice, immersed in 30% sucrose:1xPBS 4C 2h before embedding in OCT. Primary antibodies used for this study include VGLUT2 (Millipore), GFP (Aves), TagRFP (Evrogen), bgal (Abcam), myc (Millipore), HA (Sigma), Flag (Sigma), V5 (Invitrogen), Pcdhα, MOR28. In order to overcome the issue of variability in the shape, size and pattern of protoglomeruli at neonates, and potential genetic background contribution to the phenotypes we chose to asses protoglomeruli formation defects in

pairs of heterozygote vs homozygote Pcdh cluster deletion pups (preferably littermates), focusing primarily on the anterior and middle part of the olfactory bulb.

RNA FISH

Standard RNA FISH was performed as follows: fresh heads were embedded in OCT and frozen. Cryosections (18 μm) were cut and air-dried 30', fixed 10' at room temperature in 4%PFA, washed in PBS+.05% Tween-20, acetylated, blocked with hybridization solution, and hybridized overnight at 68C in hybridization solution. After extensive washing in 0.2X SSC, the slides were blocked with sheep serum, incubated with anti-Dig-AP 1:4000 (Roche) for an hour at RT and developed by 30' incubation at 37^{o} C with HNPP Fluorescent Detection Set (Roche) or BM purple. Probes were generated by RNA transcription in the presence of labeled nucleotides (Roche) from 500-800mer cDNA fragments cloned into TOPO dual promoter vector. For double fluorescent *in situs*, immunostaining was performed after ISH using standard methods as described above except that secondary antibody incubation was carried out at 4^{o}C O/N.

X-Gal Staining

Tissues were fixed for 30 min on ice with 100 mM phosphate buffer (pH 7.4), 4% paraformaldehyde, 2 mM $MgSO_4$, and 5 mM EGTA; washed with PBS and 2 mM $MgSO_4$. The blue precipitate was generated by exposure in the dark at 37°C to reaction buffer (2 mM $MgCl_2$, 0.01% sodium desoxycholate, and 0.02% Nonidet P40), with 35 mM potassium-ferricyanide, 35 mM potassium-ferrocyanide, and 1 mg/ml of X-Gal) for 2-4 hours.

Olfactometry

Mice were adapted to a reverse 12 hr light/dark cycle and water restricted (~1–1.5 ml per day to maintain 85%–90% of baseline weight) for 1 week prior to training and testing. Training and testing were performed using the Slotnick operant conditioning paradigm(*28*) and a liquid-dilution, eight-channel olfactometer (Knosys, Lutz, FL), similar to what was previously described in (*29*). Water-restricted animals were trained to lick water from a spout in response to an odor (conditioned stimulus). Next, the trained mice were directly tested in an odor discrimination assay in which they were randomly exposed to odor they were conditioned to or to a novel odor for 10 sets (BLOCKS) of 20 trials each. Each experiment consisted of 200 odor presentations. We measured the ability of control and uni-identity mice to learn to lick the spout repeatedly only in response to the conditioned odor 1 (which was followed by a water reward), and to stop licking in the presence of the novel odor, which was not followed by a reward (unconditioned stimulus). As a readout for this assay we used the number of licks during a 2s interval following the odor pulse. All odorants were purchased from Sigma-Aldrich (highest grade available) and were dissolved in light mineral oil. The fraction of correct licks was calculated as the number of correct licks/total number of licks and averaged for mice with the same genotype. Unpaired t-test with equal SD was used to calculate p values.

Axonal Distribution Index Quantification

The area covered by axons in control and OMPitTA; UNI3 in the OB was calculated from serial sections, and 3D volumes were estimated from all of the P2 lacZ positive axons (X-Gal staining) in the medial or lateral part of each olfactory bulb. As an axonal distribution index, we defined these 3D volumes corrected for the size of each olfactory bulb. The statistical

significance was evaluated using the Mann-Whitney test. The whiskers in the box plot indicate the minimum and maximum data values.

"Stray" Axonal Segments Index Quantification

We first identify the "main" MOR28 glomerulus innervated by MOR28-UNI OSNs (as main MOR28 glomerulus we defined the glomerulus with the highest MOR28-UNI signal) in the medial and lateral parts of the olfactory bulb. We then quantified any MOR28-UNI signal (axonal segments) outside of that main glomerulus. As "stray" axonal segments index we define the ratio between the number of MOR28-UNI axons (axonal segments) found outside vs inside of the main MOR28 glomerulus. The statistical significance was evaluated using the Mann-Whitney test.

In utero OE electroporation

The protocol for *in utero* cortical electroporation was modified and adapted for the OE (*30*). A mix of endotoxin-free plasmid preparation (scramble shRNA VENUS) was injected into one the olfactory epithelium of E13.5 embryos using a Picospritzer. Electroporation was performed with gold paddles to target OSNs by placing the anode (positively charged electrode) on the side of DNA injection and the cathode on the other side of the head. Four pulses of 36V for 50 ms with 500 ms interval were used for electroporation. Animals were euthanized immediately after birth.

Evaluation of Axon Arbors

Axonal arbors were evaluated for the number of branch points and total length of branches as previously described (*31*). The total length of branches (in μm) was measured as the total length of all branches from the first identified branch point, using the software NeuroJ. The 2D arbor distribution values were measured from z-stack images in each genotype using Fiji. The statistical significance was evaluated using the Kruskal-Wallis test. A minimum of $n \geq 18$ axonal arbors from control and n= 32 from mutant animals ($n \geq 6$ pups per genotype) were evaluated. In order to account for potentially confounding influences related to the location of the examined OSNs in the olfactory epithelium and the location of their projections to the OB, we sampled from the entire bulb without spatial bias.

Expression Analysis of OSNs

OSNs were sorted as described previously (*32*). RNA isolation from FACS sorted MOR28 OSNs was performed using the ARCTURUS PicoPure RNA Isolation Kit (Invitrogen). Due to limited number of MOR28 OSNs, RNA was isolated from both high and low GFP+ cells combined. Libraries were prepared using either standard protocols from Illumina or the Nextera transposase-mediated method, and sequenced on the Illumina platform. Sequence reads were mapped to the mouse mm9 genome using the Tophat version 2. The mouse UCSC annotation file, downloaded from the Illumina iGenomes website, was modified specifically for the Pcdh locus such so that the variable Pcdhα and γ exons were uncoupled from the constant exons. This process, in effect, presents each variable exon in each cluster as a single gene. All other parameters were set as default. Differential expression analysis was carried out using DESeq in the Expression Plot software package.

Circos plots were generated using the Circos software package. Gene expression values in RPKM were extracted for the mouse olfactory receptors for each individual sample (OMP

tetO GFP, OMPitTA-UNI, OMPitTA-UNI ICD*Δ*) and histograms plotted for each gene.

Tophat : http://bioinformatics.oxfordjournals.org/cgi/content/abstract/btp120
ExpressionPlot : http://www.genomebiology.com/2011/12/7/R69
Circos : http://genome.cshlp.org/content/19/9/1639

Heat map charts were generated based on previously published single OSN RNA-Seq data (*14, 15*), identifying all variable Pcdh exons that displayed CPM and RPKM values.

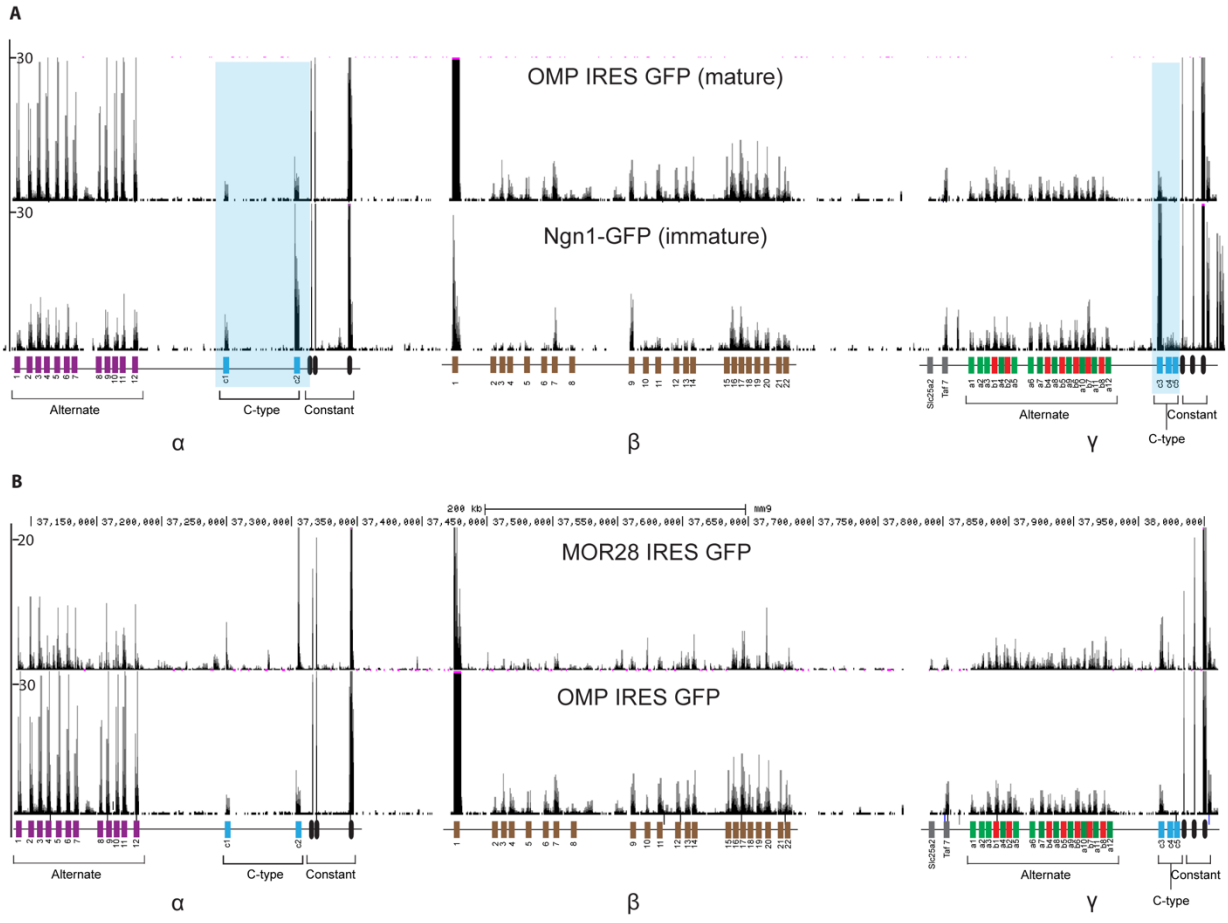
A
30
OMP IRES GFP (mature)
30
Ngn1-GFP (immature)
Alternate
C-type
Constant
α
β
Alternate
Constant
C-type
γ
B
200 kb
mm9
20
MOR28 IRES GFP
30
OMP IRES GFP
Alternate
C-type
Constant
α
β
Alternate
Constant
C-type
γ
C
Olfactory Bulb
Glomeruli (Coronal Section)
A
P
Glomeruli
D
Pcdhγ:: GFP
OB
GFP
Glomeruli
panPcdhα
Merged

Fig. S1. Expression of clustered Pcdh mRNAs and protein isoforms in OSNs.
(A) Pcdh RNA transcripts in bulk FACS sorted for OMP+ (top) or Ngn1+ (bottom) OSNs. Pcdh C-types (αc1, αc2, γc3, γc4, γc5) isoform mRNAs (highlighted with light blue) are downregulated during the differentiation of OSNs. The C-type mRNAs dominate in immature OSNs (Ngn1-GFP)(*29*), while variable isoform mRNAs dominate in mature OSNs (OMP IRES GFP). This difference is even more dramatic when OMP+ OSNs were examined at the single cell level (Table S1 & S2). **(B)** Pcdh RNA transcripts in bulk FACS sorted for MOR28+ (top) and OMP+ (bottom) OSNs. Note that both MOR28+ and OMP+ OSNs display similar patterns of Pcdh expression, showing that Pcdh expression is not coupled with OR choice. The Y axis represents the number of normalized reads. OMP: olfactory mature protein. Ngn1: Neurogenin 1. MOR28 is an olfactory receptor. **(C)** Schematic illustrating the appearance of glomeruli in a whole mount view, and in coronal sections of the OB. Glomeruli are indicated by arrows.
(D) IHC detection of GFP and all Pcdhα isoforms and merged signal in coronal sections through the olfactory bulb of Pcdhγ::GFP mice (10). The dashed circle depicts glomeruli. The dashed line designates the separation of the nerve layer (NL) and glomerular layer (GL). All sections are counterstained with Dapi (blue). Scale bar: 100μm.

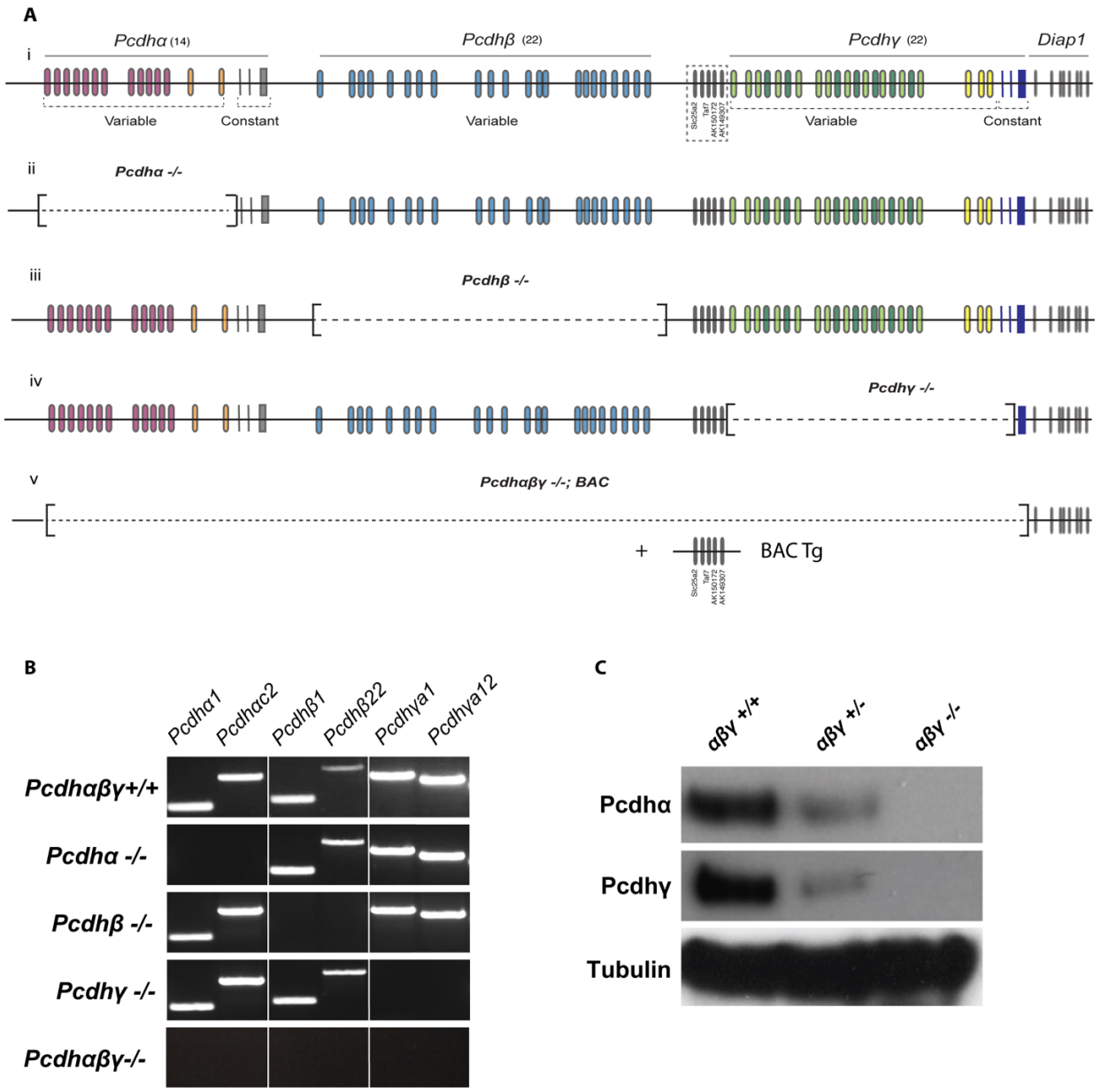

Fig. S2. Pcdh gene cluster deletions.

(A) A schematic diagram of the *Pcdh* gene cluster (i) and the deletion mutants generated in this study. *Pcdhα -/-* (ii), *Pcdhβ -/-* (iii), and *Pcdhαβγ -/-* (v). The *Pcdhγ -/-* (iv) was previously described(*9*). The four non-Pcdh genes (*Slc25a2*, *Taf7*, *AK150172*, *AK149307*) located between the *Pcdhβ* and *Pcdhγ* gene clusters are indicated by stippled box. A transgenic mouse bearing a bacterial artificial chromosome (BAC) containing the essential non-Pcdh genes was generated. These mice where crossed with of *Pcdhαβγ +/-* to rescue the early embryonic lethality of homozygous tricluster deletion mice. As expected from the phenotype of *Pcdhγ -/-* mice, *Pcdhαβγ -/-;* BAC mice die at P0. **(B)** Documentation of the genotypes of each of the deletions used in this study for each genotype by genomic PCR. **(C)** Western blot probing the expression of Pcdh protein isoforms in whole brain lysate from the *Pcdhαβγ +/+;* BAC*, Pcdhαβγ +/-;* BAC *and Pcdhαβγ -/-;* BAC pups.

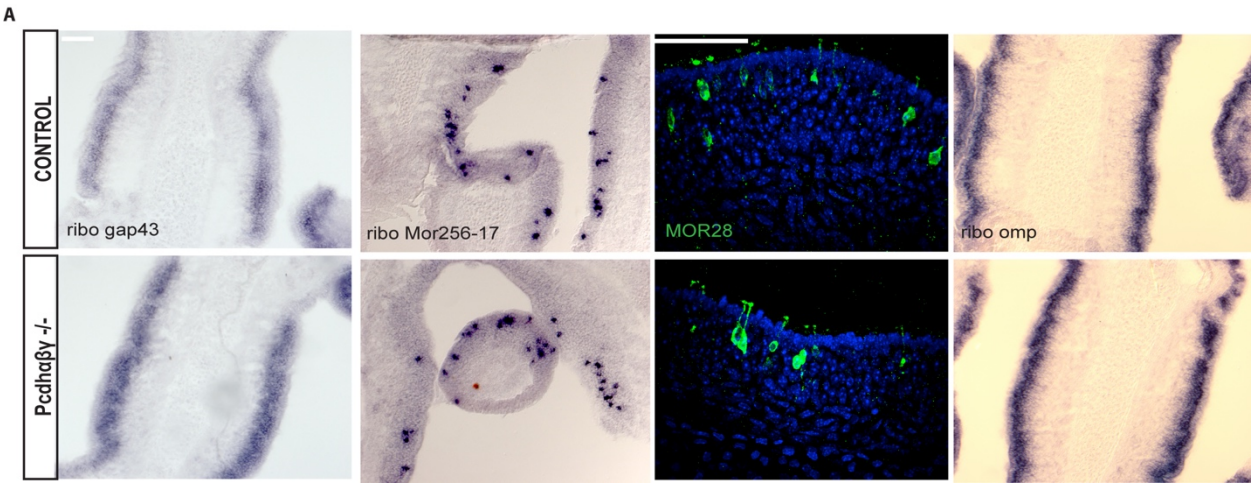

Fig S3. Normal OSN differentiation in tricluster deletion mice.
(A) RNA in situ hybridization against Gap43 (immature OSN marker), MOR256-17 (olfactory receptor), and OMP (mature OSN marker) transcripts carried out on coronal sections of the OE in control, and *Pcdhαβγ* -/- mice. IHC against MOR28 (olfactory receptor) carried out on coronal sections of the OE in control and *Pcdhαβγ* -/- P0 mice. We note that Gap43 signal appeared slightly increased in the tricluster deletion mice. However, no other significant difference was observed between control and tricluster mutant mice. All control and tricluster deletion animals also express the BAC transgene. Scale bar: 254μm and 100μm.

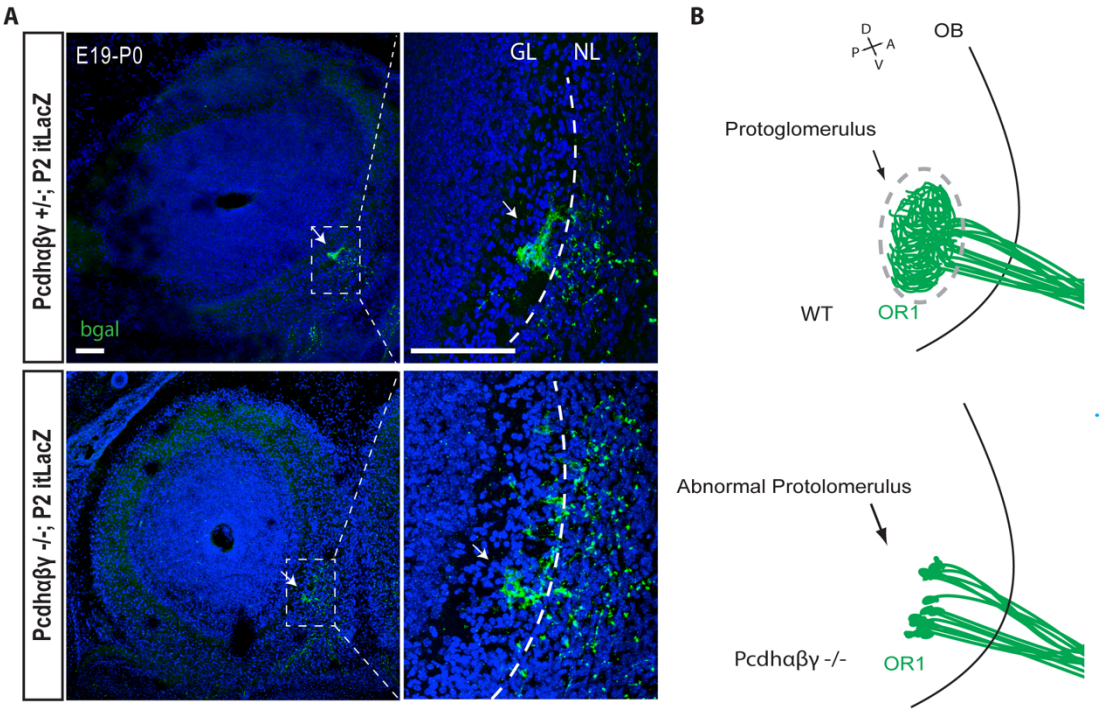

Fig. S4. OSN axons expressing the same OR form aberrant protoglomeruli in Pcdh tricluster deletion mutants.
(A) IHC against bgal in coronal sections of the OB of *Pcdhαβγ +/-;* P2 itLacZ and *Pcdhαβγ -/-*; P2 itLacZ E19-P0 embryos. Note that P2 axons project to approximately the same medial ventral location in the OB of both mutant and control mice. The dashed line designates the approximate separation of the nerve layer (NL) and the glomerular layer (GL). White arrows depict the P2 protoglomerulus (n≥3). All sections were counterstained with Dapi (blue). All control and tricluster deletion animals also express the BAC transgene. **(B)** A schematic illustration of OSN axons expressing a single OR ("like" axons), as they converge to form a protoglomerulus in the olfactory bulb in WT (top) and *Pcdhαβγ -/-* (bottom) P0 mice. In the absence of all Pcdh proteins, like OSNs form abnormal protoglomeruli due to their defective axonal arborization caused by clumping (see also Fig. S5). The grey dashed circle designates the approximate location in the OB where a protoglomerulus is formed. Scale bar: 100μm.

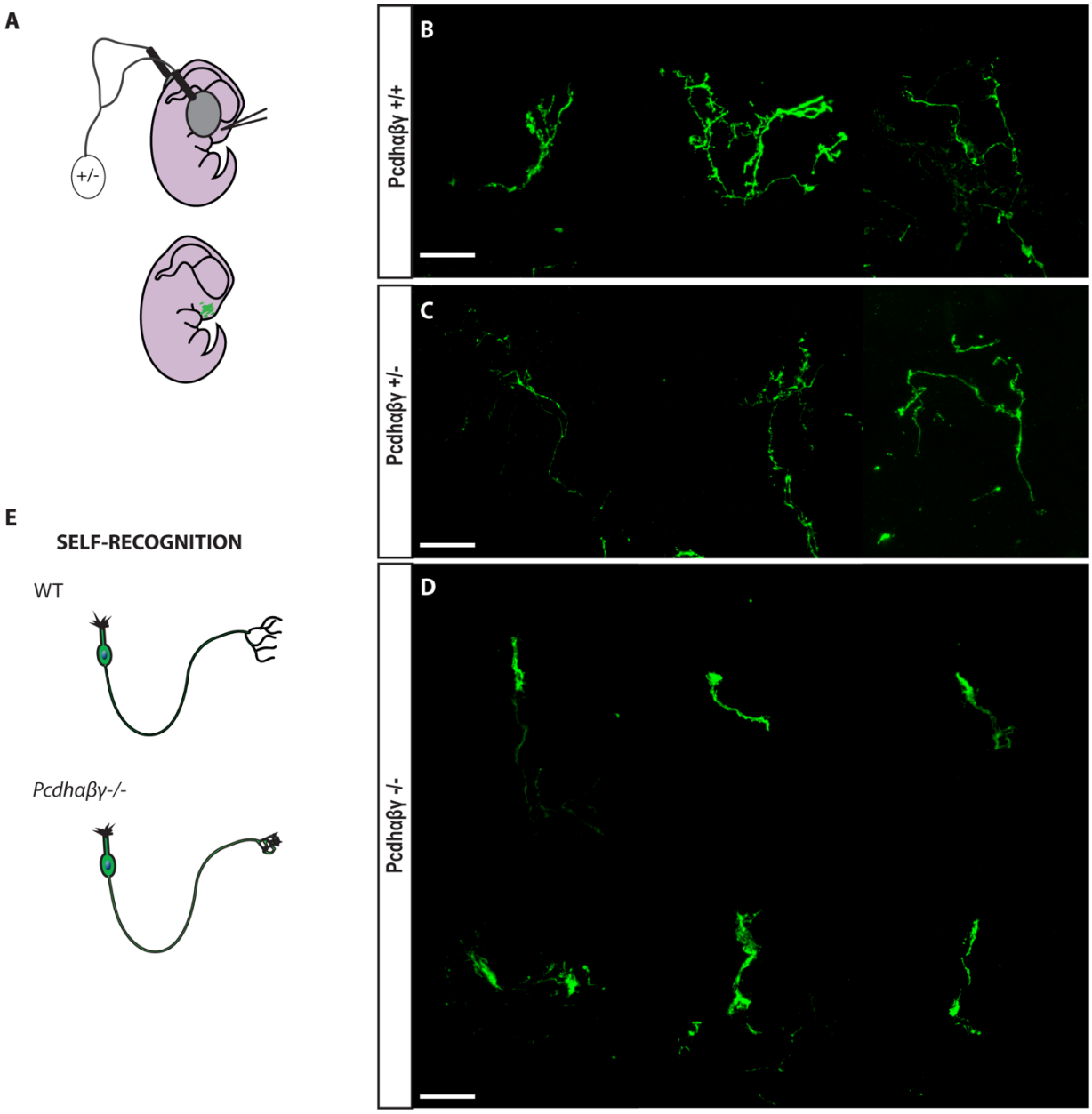

Fig. S5. OSN axonal arborization is disrupted in Pcdh tricluster deletion mice.
(A) Schematic showing the *in-utero* electroporation method (see Material and Methods for details). IHC against Venus in the in utero electroporated OSNs from *Pcdhαβγ +/+* **(B)**, *Pcdhαβγ +/-* **(C)** and *Pcdhαβγ -/-* **(D)** E19-P0 mice. **(E)** Proposed model to explain the axonal arborization defect: normally, single pioneer OSNs send axons that branch (top) in the OB. However, in the absence of Pcdhs, the loss of self-recognition results in the collapse of axonal arbors (bottom). All control and tricluster deletion animals also express the BAC transgene. Scale bar: 20μm.

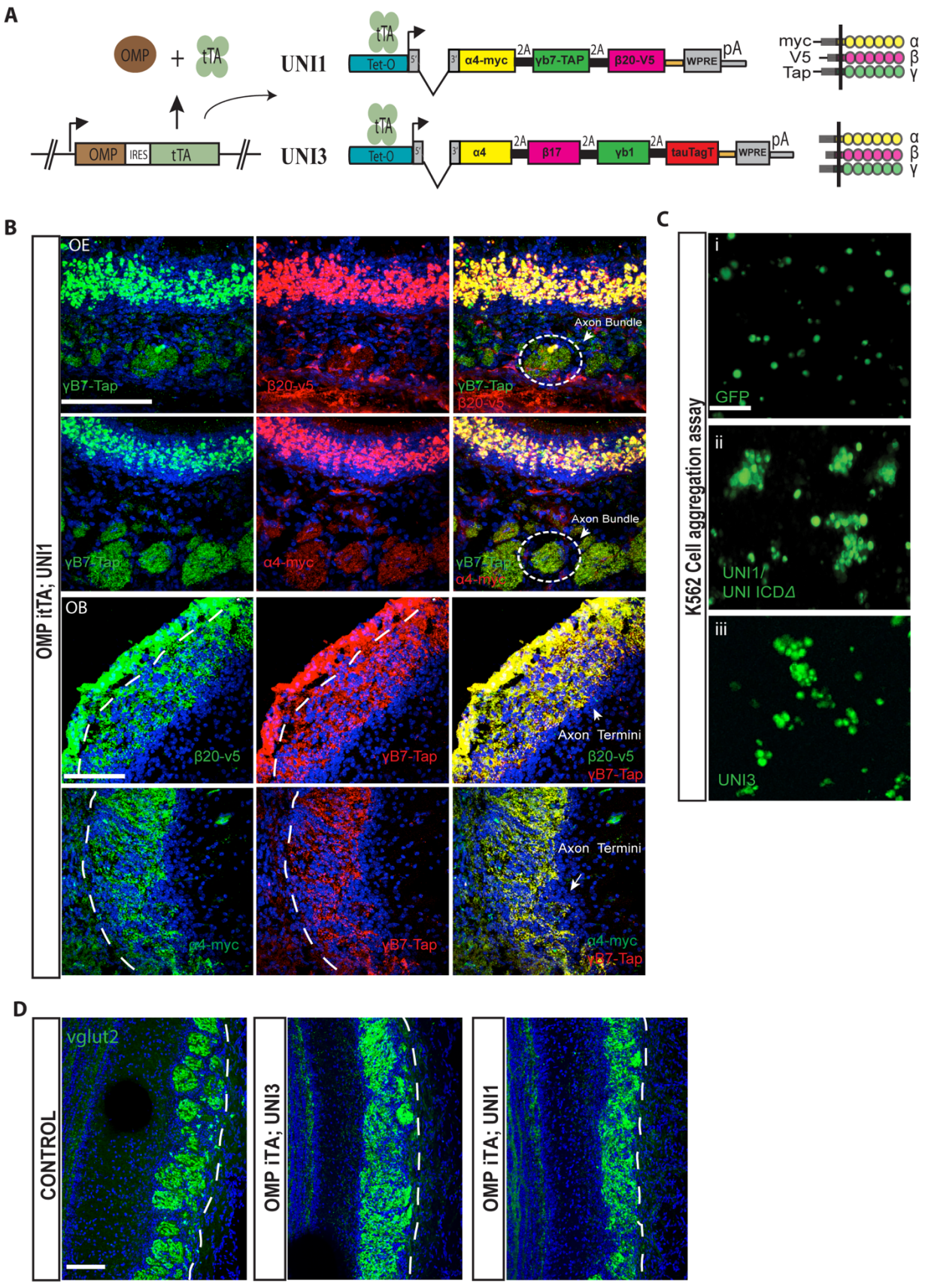
A
OMP
tTA
UNI1
Tet-O
α4-myc
2A
γb7-TAP
β20-V5
WPRE
pA
myc
V5
Tap
α
β
γ
OMP
IRES
tTA
UNI3
α4
β17
γb1
tauTagT
B
OMP iTA; UNI1
OE
γB7-Tap
β20-v5
Axon Bundle
α4-myc
OB
Axon Termini
C
K562 Cell aggregation assay
i
GFP
ii
UNI1/
UNI ICDΔ
iii
UNI3
D
CONTROL
vglut2
OMP iTA; UNI3
OMP iTA; UNI1

Fig. S6. Expression of uni-identity Pcdhs disrupts the formation of glomeruli.
(A) A schematic of the genetic strategy used to override the endogenous multi-cluster Pcdh single cell diversity by expressing high levels of three Pcdh isoforms (α & β & γ) exclusively in mature OSNs. OSN neuron-specific driver (OMP itTA) to express the same set of arbitrarily chosen Pcdh protein isoforms in mOSNs, at the time in development at which their axons normally converge to form glomeruli in the olfactory bulb (*33*) **(B)** IHC detection of Pcdhγb7-Tap, Pcdhβ20-V5 and Pcdhα4-myc in coronal sections through the OE in OMPitTA; UNI1 mice. The dashed circle depicts axonal bundles of OSNs from OMPitTA; UNI1 mice. IHC detection of Pcdhβ20-V5, Pcdhγb7-Tap and Pcdhα4-myc in a coronal section through the OB in OMPitTA; UNI1 mice. As expected, all uni-Pcdh isoforms co-localized in the soma and axons of OSNs in uni-identity mice. **(C)** UNI1/ICDΔ or UNI3 engage in homophilic interactions in the K562 cell aggregation assay (*2, 3*) . K562 cells were transfected with the UNI1/ ICDΔ or the UNI3 expressing construct. After 24 hours, the transfected cells were allowed to aggregate (K562 cells normally do not aggregate). K562 aggregates were induced only by uni-Pcdh expression and not with the expression of a control cassette (expressing only GFP). **(D)** IHC against vesicular glutamate transporter 2 (vglut2) in coronal sections through the OB of control, OMPitTA; UNI1 and OMPitTA; UNI3 mice. Note the absence of distinct glomeruli in uni-identity adult mice compared to control adult mice. The dashed line designates the separation of the NL and the GL. All sections are counterstained with Dapi (blue). Scale bar: 100μm.

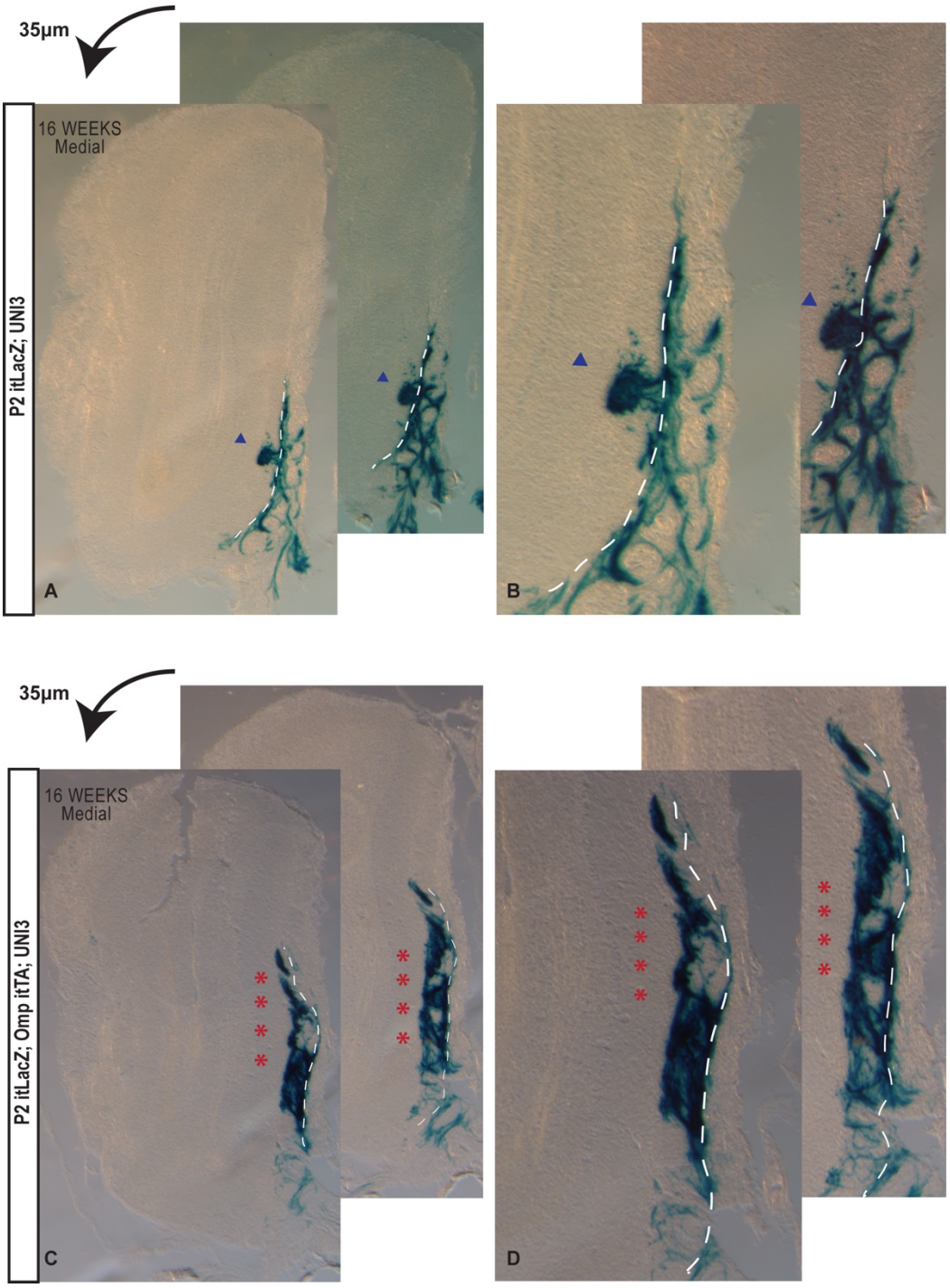

Fig. S7. Uni-identity OSNs display axonal convergence defects.
X-Gal staining in coronal serial sections (35µm) through the whole (left panel) and zoomed in area (right) of OB, from control **(A-B)** and OMP itTA; UNI3; P2 itLacZ **(C-D)** 16 week mice. The dashed line designates the separation of the NL and the GL. Arrows indicate the P2 glomerulus. Asterisks indicate the mutant P2 axonal projections in uni-identity mice. Similar results were obtained for both the medial and lateral side of the OB.

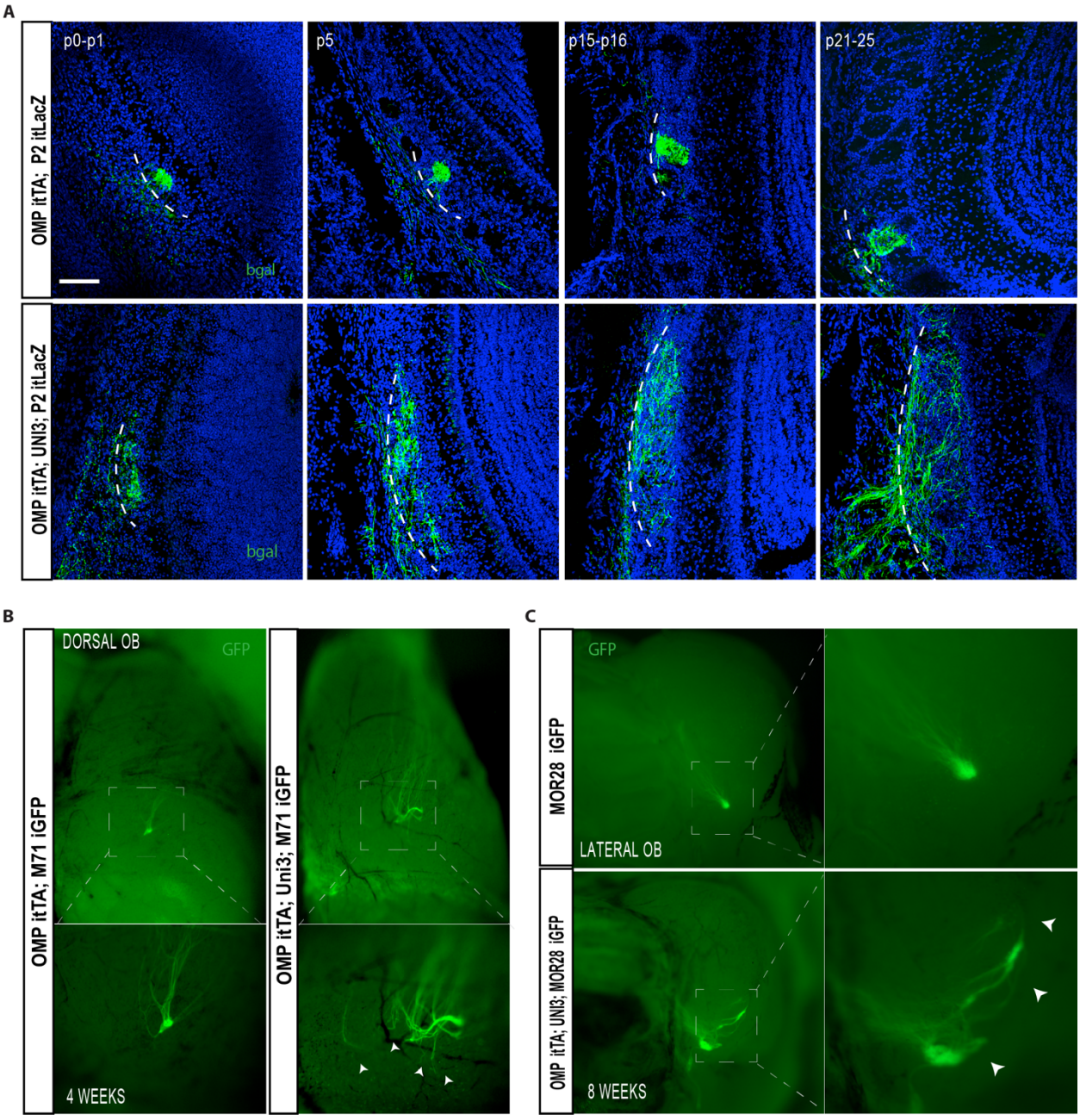

Fig. S8. Uni-identity OSNs display axonal convergence defects.
(A) Developmental time course of P2 OSN axons stained by IHC against bgal in coronal sections through the OB from control and OMP itTA; UNI3; P2 itLacZ mice. The dashed line designates the separation of the NL and the GL. bgal is pseudo-colored green. All sections were counter stained with Dapi (blue). **(B)** Whole-mount staining of OB reveals M71 itGFP dorsal axonal projections in control and OMPitTA; UNI3 animal. **(C)** Whole-mount staining of OB reveals MOR28 itGFP ventral/lateral axonal projections in control and in a OMP itTa; UNI3 animal. Arrows indicate stray OSN axons. Scale bar: 100µm.

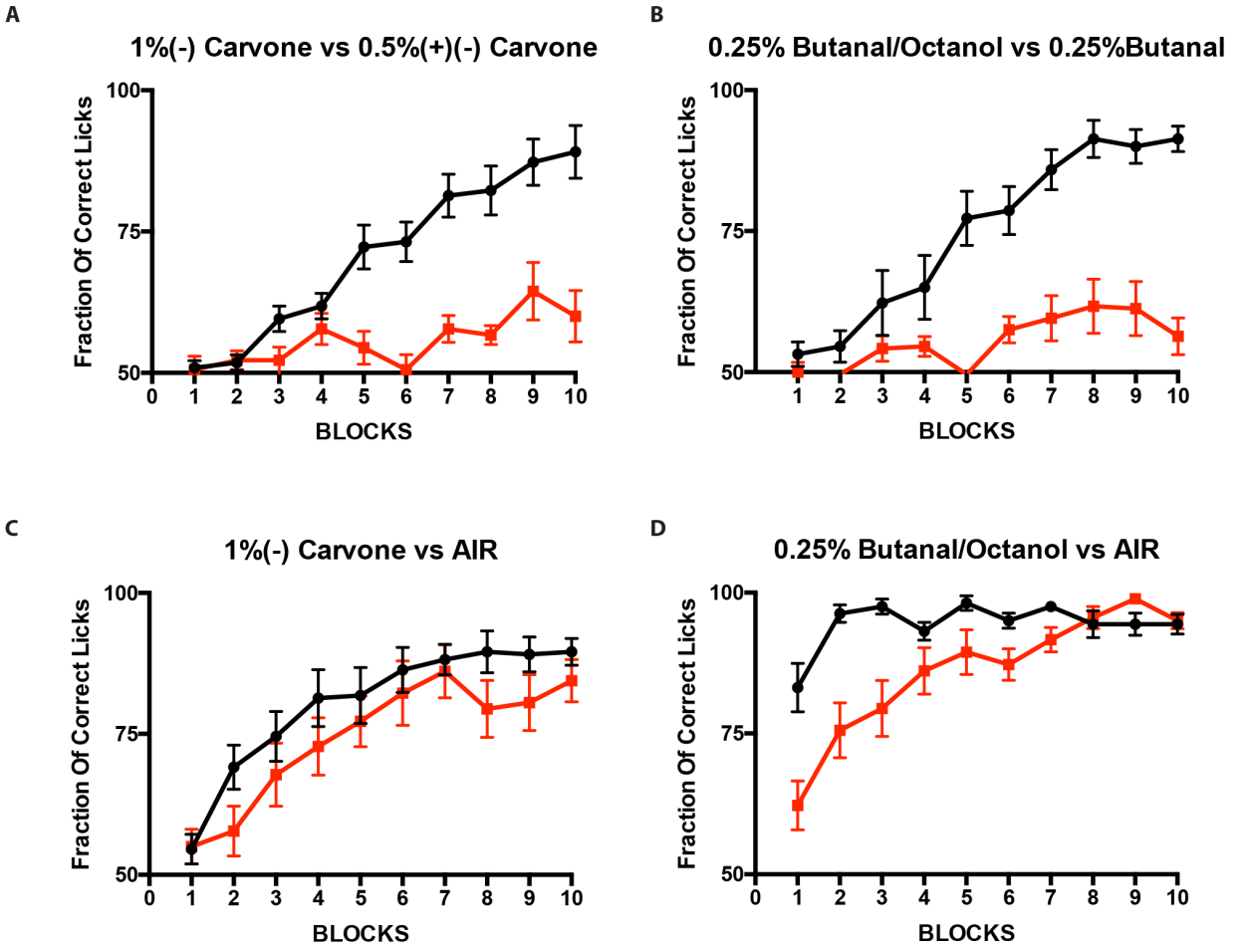

Fig. S9. Uni-identity mice display odor discrimination defects.
(A) Control mice (black) can discriminate between 1% (-) carvone and a mixture of 0.5% (+)/(-) carvone enantiomers. However, uni-identity animals (red) fail to discriminate (-) carvone from a mixture of the enantiomers. (n≥9; Unpaired t-test with equal SD, p=0.0045). **(B)** Uni-identity animals fail to discriminate a mixture of 0.25% butanal / 0.25% octanol from 0.25% butanal (n≥9; Unpaired t-test with equal SD, p=0.0011). **(C-D)** The same control (black) and uni-identity (red) animals can detect 1% (-) carvone and 0.25% butanal / 0.25% octanol respectively (n≥9). The fraction of correct licks in response to rewarded (with water) versus unrewarded odor is shown. Animals were considered to be capable of discriminating the two neutral odors if the fraction of correct licks is ≥ 75%-80% for at least three consecutive trials. 5-12 months old transgenic animals were used (see Material and Methods for detailed description of the behavioral assay). Error bars represent SEM.

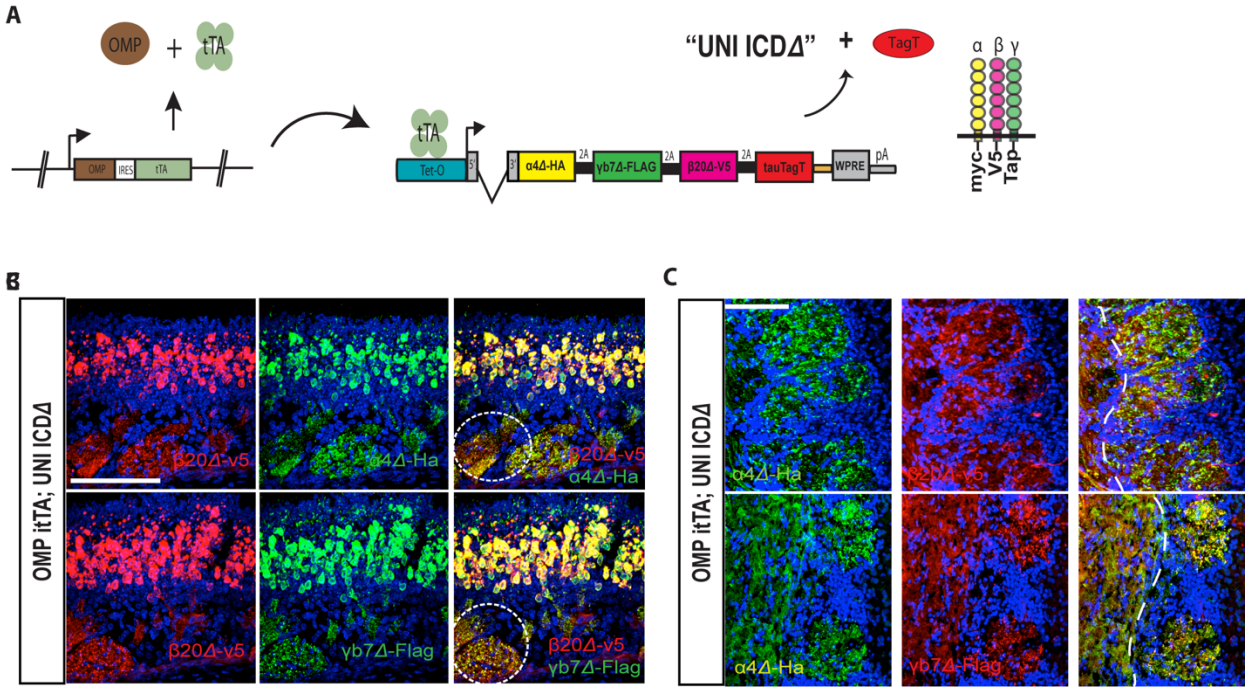

Fig. S10. UNI ICDΔ+ OSNs form glomeruli.
(A) Schematic of the genetic strategy used to express the UNI ICDΔ Pcdh combinations (truncated Pcdhα, Pcdhβ & Pcdhγ proteins lacking the intracellular domains) in all mature OSNs. **(B)** IHC detection of Pcdhβ20Δ, Pcdhα4Δ and Pcdhγb7Δ isoforms in coronal sections through the OE in OMPitTA; Uni ICD*Δ* mice. The dashed circle depicts axonal bundles of OSNs in OMPitTA; Uni ICDΔ mice. **(C)** IHC detection of Pcdhα4Δ, Pcdhβ20Δ and Pcdhγb7Δ isoforms in coronal sections through the OB in OMPitTA; UNI ICDΔ mice. The dashed line designates the separation of NL and the GL. bgal is pseudo-colored in green. Animals were 4 weeks old. All sections were counterstained with Dapi (blue). Scale bar: 100µm.

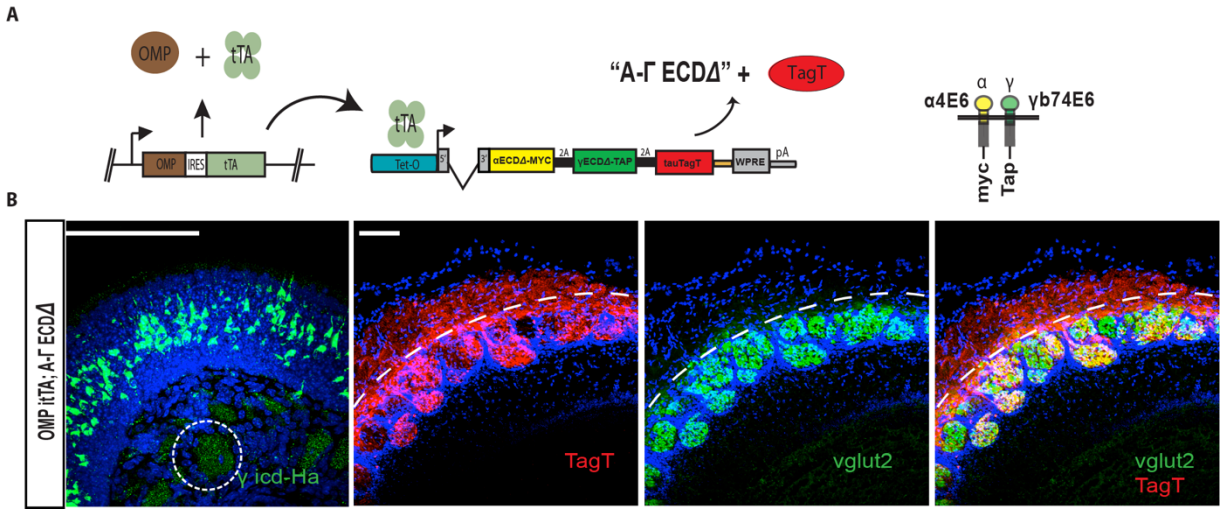

Fig. S11. A-Γ ECDΔ + OSNs form normal appearing glomeruli.
(A) Schematic of the genetic strategy used to express the A-Γ ECDΔ Pcdh combinations (truncated Pcdhα and Pcdhγ proteins that lack the extracellular domains EC1-EC5 required for trans-interactions (3)) in all mature OSNs. **(B)** IHC detection of the Pcdhγ ICD in coronal sections through the OE in OMPitTA; A-Γ ECDΔ mice. IHC against TagT and vglut2 in coronal sections through the OB of control, OMPitTA; A-Γ ECDΔ 4 weeks old mice. The dashed circle depicts axonal bundles of OSNs in OMPitTA; A-Γ ECDΔ mice. Dashed line designates the separation of NL and the GL. All sections were counterstained with Dapi (blue). Scale bar: 100µm.

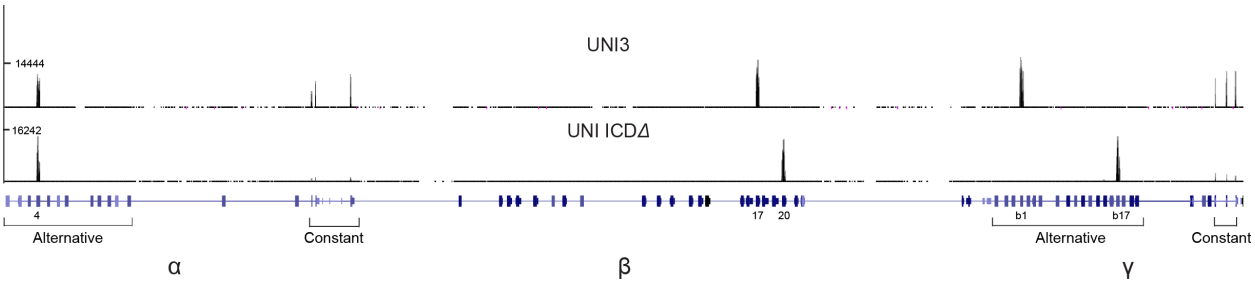

Fig. S12. Expression of exogenous Pcdhs in FACS sorted UNI3+ and UNI ICDΔ+ OSNs. Raw RNA-Seq reads for Pcdh RNA expression from bulk FACS sorted mature OSNs positive for UNI3 and UNI ICDΔ expression. Note that in each sample the levels of exogenous Pcdhα, β and γ mRNAs are orders of magnitude higher than those of the endogenous Pcdh mRNAs (which are not visible any more).

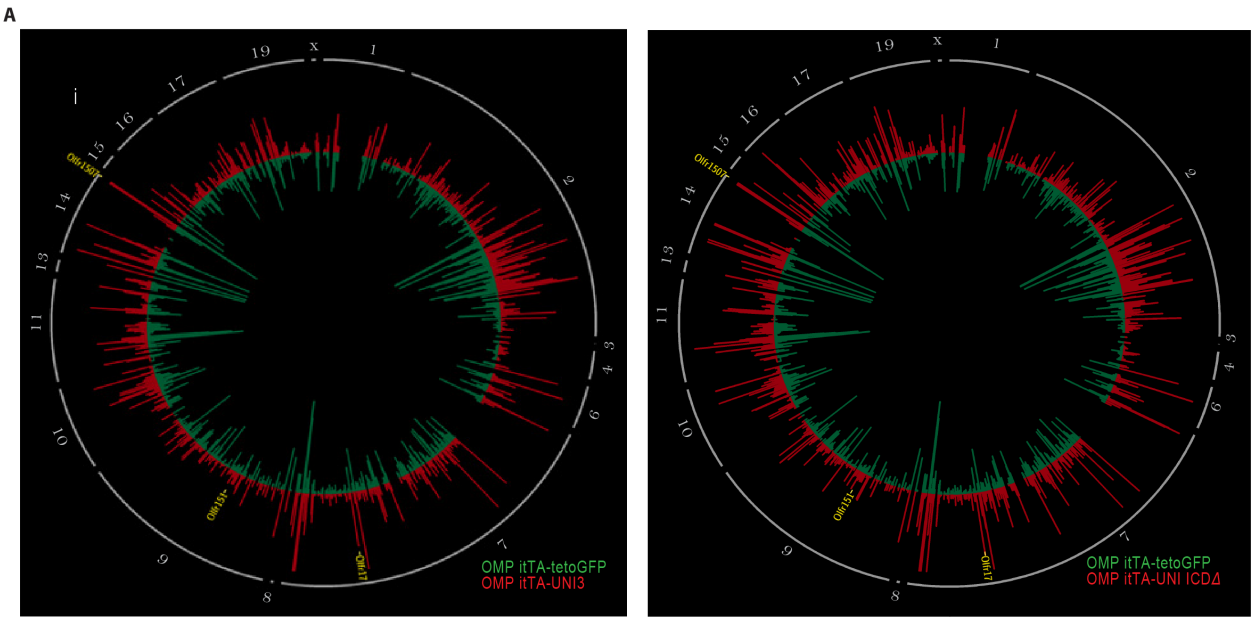

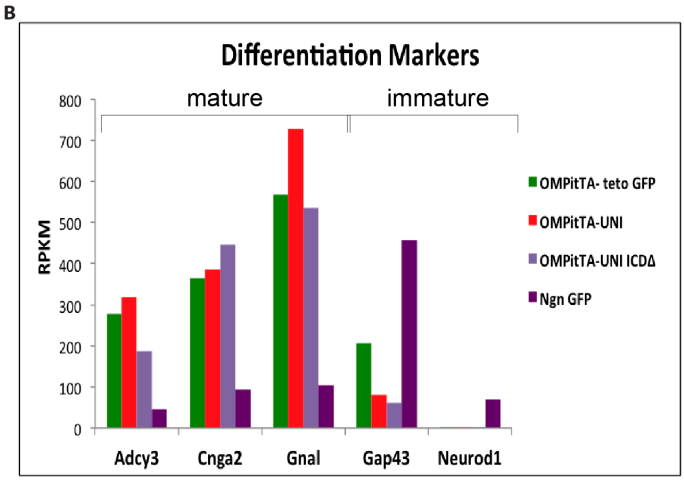

Fig. S13. OR expression is unaffected in uni-identity mice.
(A) RPKM levels for each Ref-Seq OR in the mouse genome from FACS sorted mature OSNs expressing GFP (green), UNI3 (red) or UNI ICDΔ (red). Note that the RNA expression of ORs is similar in mutants and controls. External grey ring numbers represents relative chromosomal locations of each OR gene. The P2 (*olfr17*), M71 (*olfr151*) and MOR28 (*olfr1507*) olfactory receptor genes are depicted with yellow. **(B)** RPKM levels of developmental markers in FACS sorted mature OSNs expressing GFP, UNI3 or UNI ICDΔ and immature OSNs (Ngn-GFP). Note that OSNs expressing GFP, UNI3 or UNI ICDΔ construct maintain their mature differentiation status (high levels of *Adcy3*, *Cnga2*, *Gnal*).

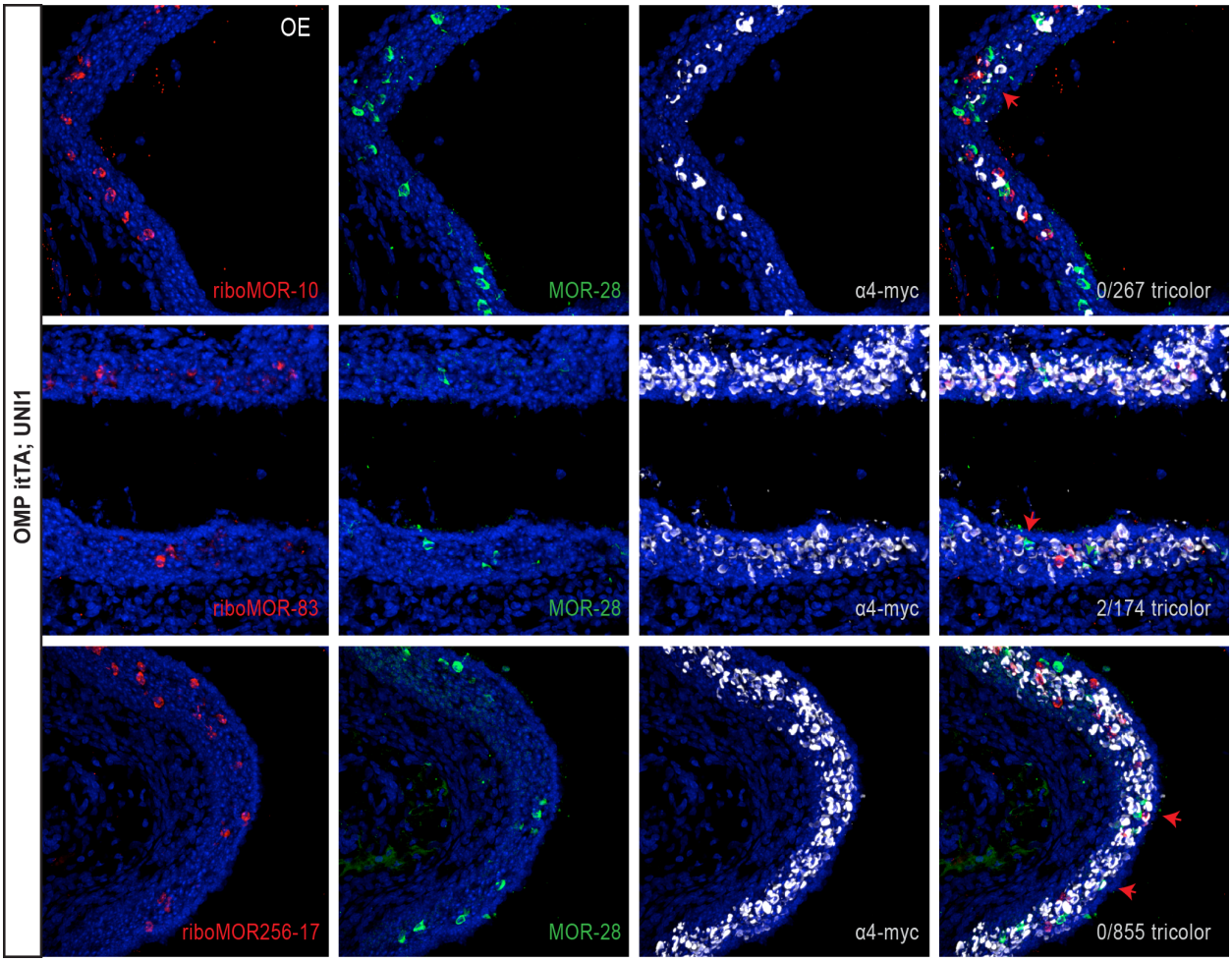

Fig. S14. The stability of OR choice is unaffected in uni-identity mice.
We hypothesized that if OR choice is destabilized we should be able to detect more than one OR in OSNs from OMPitTA; UNI1 mice. RNA fluorescence *in situ* hybridization followed by double IHC staining carried out on the OE of OMPitTA; UNI1 mice. Using RNA probes against other ORs such as MOR10, MOR83 (same genomic cluster as MOR28) and MOR256-17 (different genomic cluster from MOR28) we asked whether we could detect these transcripts in MOR28+/UNI1+ OSNs. We were unable to detect any MOR28+/UNI+ OSNs expressing the MOR10 and MOR256-17 ORs in coronal sections of the OE in 4 weeks OMPitTA; UNI1 mice. Similarly, the vast majority of MOR28+/UNI+ OSNs did not express the MOR83 OR. Signals from *in situ* and antibody staining are merged in the last column of panels. MOR28 expressing UNI1 OSNs are shown with red arrows. Sections are counterstained with Dapi (blue). Scale bar: 100μm.

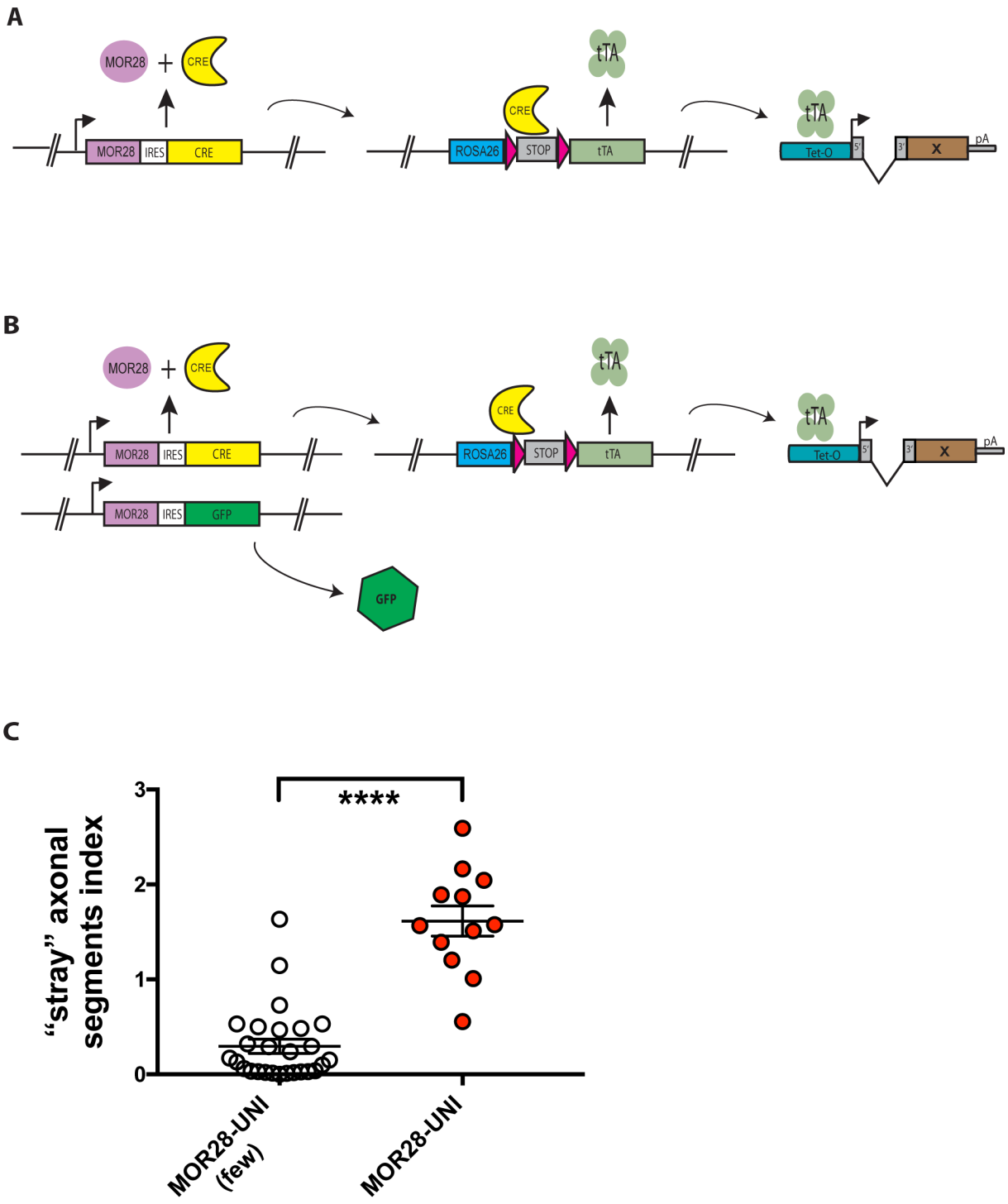

Fig. S15. The strategy to override endogenous Pcdh diversity exclusively in MOR28 like OSNs.

(A) A schematic showing the genetic strategy used to drive the expression of X= GFP or UNI3 or UNI ICDΔ exclusively in MOR28 OSNs. **(B)** A Schematic showing the genetic strategy used to drive the expression of UNI3 in only a small population of MOR28 OSNs. Because of the monogenic and monoallelic expression of OR genes, heterozygous mice for the MOR28 iCRE

and MOR28 iGFP alleles are expected to produce similar numbers of MOR28 OSNs that express either X= UNI3+, or GFP+ (wild type), but never both. We note however, that the number of MOR28-UNI3 OSNs were to our advantage, much lower than their counterparts expressing GFP, presumably due to inefficient Cre-dependent induction of uni-Pcdh expression. **(C)** Quantitation of "stray" MOR28-UNI axons in mice with few (white circles) or with many MOR28-UNI axons (red circles). As "stray" axonal segment index we defined the ratio of MOR28-UNI axons (axonal segments) that "stray" off the site of the main MOR28 glomerulus formation in both the medial and lateral regions of each bulb. Indeed, we found that by increasing the numbers of MOR28-UNI OSNs, the converging defects in each part of the olfactory bulb are significantly exacerbated. Error bars represent SEM. ($n \geq 3$ animals per genotype; Mann-Whitney *U*-Test, $p < 0.0001$).

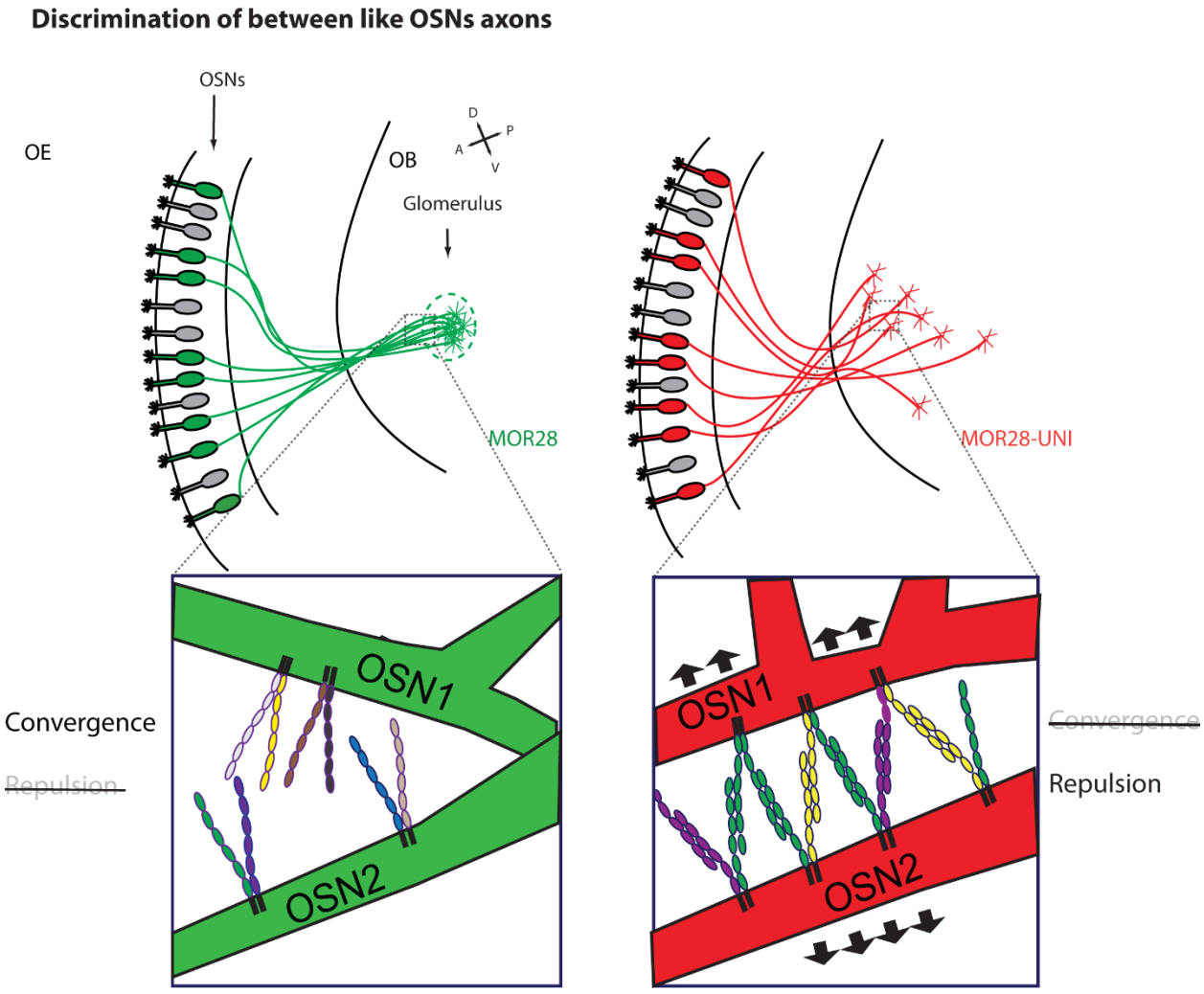

Fig. S16. Proposed model for the role of Pcdh mediated diversity in glomeruli formation During the first postnatal week of development, large numbers of OSN axons converge to form glomeruli in the olfactory bulb. In wild type animals, individual OSNs with the same OR, stochastically express random sets of Pcdh isoforms from all three gene clusters (depicted by different colors), which assemble into homo and hetero cis-dimers that fail to engage in homophilic interactions at the cell surface. In the absence of these interactions and the associated repulsion, OSN axons converge to form glomeruli (left). By contrast, we propose that in uni-identity mice, where like-OSNs display a single dominant Pcdh identity, axons fail to converge because of the contact-dependent repulsion mediated by the uni-Pcdhs.

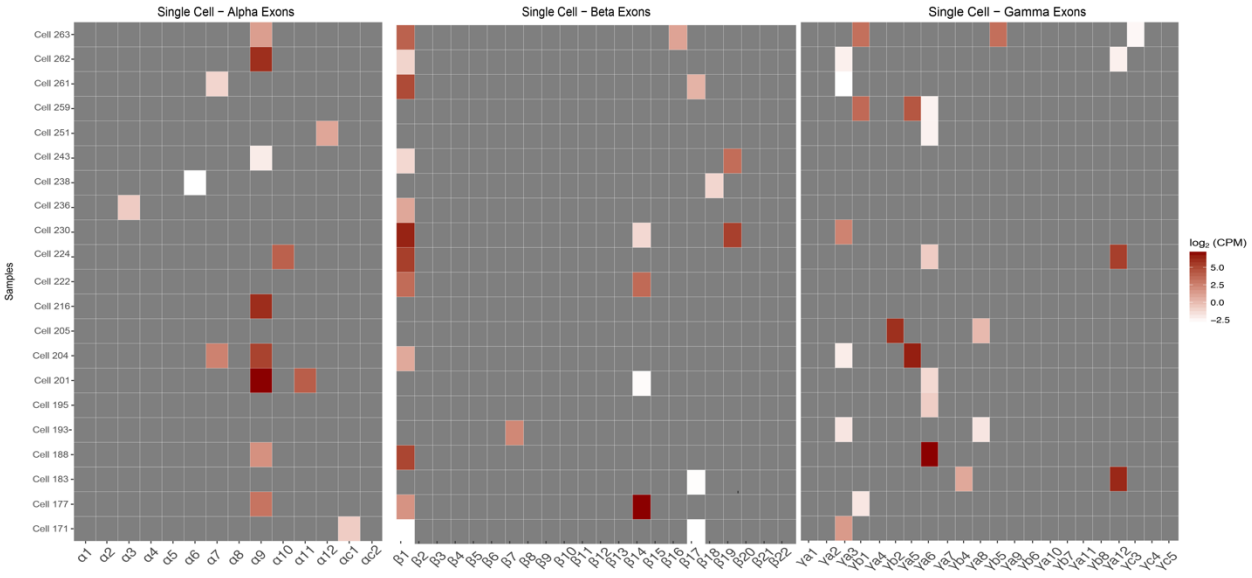

Table S1. Single OSNs express unique repertoires of Pcdh mRNAs from all three clusters. Pcdh transcripts from individual mature OSNs (16). Note that the majority of cells stochastically express isoforms from all three Pcdh clusters and that the C-type Pcdh isoform mRNAs (αc1, αc2, γc3, γc4, γc5) are strikingly under-represented in mature OSNs. The presence of individual Pcdh isoforms mRNA is indicated by the red colored boxes, and the levels are indicated by the color gradient (log2 CPM).

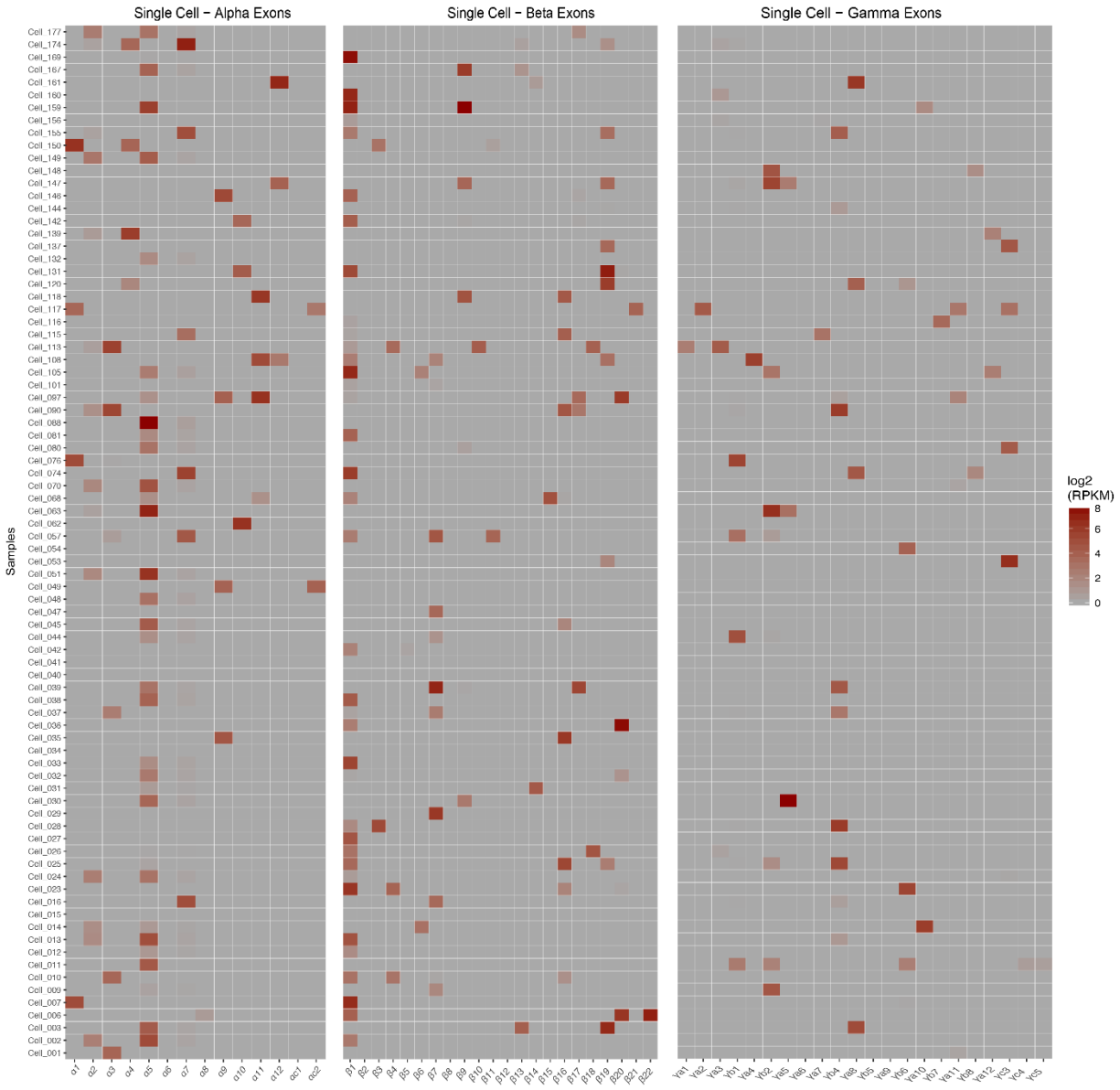

Table S2. Single OSNs express unique repertoires of Pcdhs mRNAs from all three clusters. Pcdh transcripts from individual mature OSNs that express ORs (17). Note that the majority of cells express isoforms from all three Pcdh gene clusters and that the C-type Pcdh isoform mRNAs (αc1, αc2, γc3, γc4, γc5) are strikingly under-represented in mature OSNs. Pcdh transcripts were not detected in 6% of the cells, presumably due to inadequate sequencing depth. The presence of individual Pcdh isoforms mRNA is indicated by the red colored boxes, and the levels are indicated by the color gradient (log2 RPKM).

References

1. B. Tasic, C. E. Nabholz, K. K. Baldwin, Y. Kim, E. H. Rueckert, S. A. Ribich, P. Cramer, Q. Wu, R. Axel, T. Maniatis, Promoter choice determines splice site selection in protocadherin α and γ pre-mRNA splicing. *Mol. Cell* **10**, 21–33 (2002). doi:10.1016/S1097-2765(02)00578-6 Medline

2. X. Wang, H. Su, A. Bradley, Molecular mechanisms governing *Pcdh-γ* gene expression: Evidence for a multiple promoter and cis-alternative splicing model. *Genes Dev.* **16**, 1890–1905 (2002). doi:10.1101/gad.1004802 Medline

3. R. Rubinstein, C. A. Thu, K. M. Goodman, H. N. Wolcott, F. Bahna, S. Mannepalli, G. Ahlsen, M. Chevee, A. Halim, H. Clausen, T. Maniatis, L. Shapiro, B. Honig, Molecular logic of neuronal self-recognition through protocadherin domain interactions. *Cell* **163**, 629–642 (2015). doi:10.1016/j.cell.2015.09.026 Medline

4. D. Schreiner, J. A. Weiner, Combinatorial homophilic interaction between γ-protocadherin multimers greatly expands the molecular diversity of cell adhesion. *Proc. Natl. Acad. Sci. U.S.A.* **107**, 14893–14898 (2010). doi:10.1073/pnas.1004526107 Medline

5. C. A. Thu, W. V. Chen, R. Rubinstein, M. Chevee, H. N. Wolcott, K. O. Felsovalyi, J. C. Tapia, L. Shapiro, B. Honig, T. Maniatis, Single-cell identity generated by combinatorial homophilic interactions between α, β, and γ protocadherins. *Cell* **158**, 1045–1059 (2014). doi:10.1016/j.cell.2014.07.012 Medline

6. J. L. Lefebvre, D. Kostadinov, W. V. Chen, T. Maniatis, J. R. Sanes, Protocadherins mediate dendritic self-avoidance in the mammalian nervous system. *Nature* **488**, 517–521 (2012). doi:10.1038/nature11305 Medline

7. W. V. Chen, F. J. Alvarez, J. L. Lefebvre, B. Friedman, C. Nwakeze, E. Geiman, C. Smith, C. A. Thu, J. C. Tapia, B. Tasic, J. R. Sanes, T. Maniatis, Functional significance of isoform diversification in the protocadherin gamma gene cluster. *Neuron* **75**, 402–409 (2012). doi:10.1016/j.neuron.2012.06.039 Medline

8. A. M. Garrett, D. Schreiner, M. A. Lobas, J. A. Weiner, γ-Protocadherins control cortical dendrite arborization by regulating the activity of a FAK/PKC/MARCKS signaling pathway. *Neuron* **74**, 269–276 (2012). doi:10.1016/j.neuron.2012.01.028 Medline

9. J. Ledderose, S. Dieter, M. K. Schwarz, Maturation of postnatally generated olfactory bulb granule cells depends on functional γ-protocadherin expression. *Sci. Rep.* **3**, 1514 (2013). doi:10.1038/srep01514 Medline

10. J. L. Lefebvre, Y. Zhang, M. Meister, X. Wang, J. R. Sanes, γ-Protocadherins regulate neuronal survival but are dispensable for circuit formation in retina. *Development* **135**, 4141–4151 (2008). doi:10.1242/dev.027912 Medline

11. X. Wang, J. A. Weiner, S. Levi, A. M. Craig, A. Bradley, J. R. Sanes, Gamma protocadherins are required for survival of spinal interneurons. *Neuron* **36**, 843–854 (2002). doi:10.1016/S0896-6273(02)01090-5 Medline

12. S. Hasegawa, S. Hamada, Y. Kumode, S. Esumi, S. Katori, E. Fukuda, Y. Uchiyama, T. Hirabayashi, P. Mombaerts, T. Yagi, The protocadherin-α family is involved in axonal

coalescence of olfactory sensory neurons into glomeruli of the olfactory bulb in mouse. *Mol. Cell. Neurosci.* **38**, 66–79 (2008). doi:10.1016/j.mcn.2008.01.016 Medline

13. L. Buck, R. Axel, A novel multigene family may encode odorant receptors: A molecular basis for odor recognition. *Cell* **65**, 175–187 (1991). doi:10.1016/0092-8674(91)90418-X Medline

14. A. Chess, I. Simon, H. Cedar, R. Axel, Allelic inactivation regulates olfactory receptor gene expression. *Cell* **78**, 823–834 (1994). doi:10.1016/S0092-8674(94)90562-2 Medline

15. P. Mombaerts, F. Wang, C. Dulac, S. K. Chao, A. Nemes, M. Mendelsohn, J. Edmondson, R. Axel, Visualizing an olfactory sensory map. *Cell* **87**, 675–686 (1996). doi:10.1016/S0092-8674(00)81387-2 Medline

16. L. R. Saraiva, X. Ibarra-Soria, M. Khan, M. Omura, A. Scialdone, P. Mombaerts, J. C. Marioni, D. W. Logan, Hierarchical deconstruction of mouse olfactory sensory neurons: From whole mucosa to single-cell RNA-seq. *Sci. Rep.* **5**, 18178 (2015). doi:10.1038/srep18178 Medline

17. L. Tan, Q. Li, X. S. Xie, Olfactory sensory neurons transiently express multiple olfactory receptors during development. *Mol. Syst. Biol.* **11**, 844 (2015). doi:10.15252/msb.20156639 Medline

18. S. Esumi, N. Kakazu, Y. Taguchi, T. Hirayama, A. Sasaki, T. Hirabayashi, T. Koide, T. Kitsukawa, S. Hamada, T. Yagi, Monoallelic yet combinatorial expression of variable exons of the protocadherin-α gene cluster in single neurons. *Nat. Genet.* **37**, 171–176 (2005). doi:10.1038/ng1500 Medline

19. S. Hasegawa, T. Hirabayashi, T. Kondo, K. Inoue, S. Esumi, A. Okayama, S. Hamada, T. Yagi, Constitutively expressed protocadherin-α regulates the coalescence and elimination of homotypic olfactory axons through its cytoplasmic region. *Front. Mol. Neurosci.* **5**, 97 (2012). doi:10.3389/fnmol.2012.00097 Medline

20. W. V. Chen, T. Maniatis, Clustered protocadherins. *Development* **140**, 3297–3302 (2013). doi:10.1242/dev.090621 Medline

21. T. Hummel, M. L. Vasconcelos, J. C. Clemens, Y. Fishilevich, L. B. Vosshall, S. L. Zipursky, Axonal targeting of olfactory receptor neurons in *Drosophila* is controlled by Dscam. *Neuron* **37**, 221–231 (2003). doi:10.1016/S0896-6273(02)01183-2 Medline

22. D. Hattori, E. Demir, H. W. Kim, E. Viragh, S. L. Zipursky, B. J. Dickson, Dscam diversity is essential for neuronal wiring and self-recognition. *Nature* **449**, 223–227 (2007). doi:10.1038/nature06099 Medline

23. W. V. Chen, C. L. Nwakeze, C. A. Denny, S. O'Keeffe, M. A. Rieger, G. Mountoufaris, A. Kirner, J. D. Dougherty, R. Hen, Q. Wu, T. Maniatis, Pcdhac2 is required for axonal tiling and assembly of serotonergic circuitries in mice. *Science* **356**, 10.1126/science.aal3231 (2017).

24. C. R. Yu, J. Power, G. Barnea, S. O'Donnell, H. E. V. Brown, J. Osborne, R. Axel, J. A. Gogos, Spontaneous neural activity is required for the establishment and maintenance of the olfactory sensory map. *Neuron* **42**, 553–566 (2004). doi:10.1016/S0896-6273(04)00224-7 Medline

25. B. M. Shykind, S. C. Rohani, S. O'Donnell, A. Nemes, M. Mendelsohn, Y. Sun, R. Axel, G. Barnea, Gene switching and the stability of odorant receptor gene choice. *Cell* **117**, 801–815 (2004). doi:10.1016/j.cell.2004.05.015 Medline

26. P. Feinstein, P. Mombaerts, A contextual model for axonal sorting into glomeruli in the mouse olfactory system. *Cell* **117**, 817–831 (2004). doi:10.1016/j.cell.2004.05.011 Medline

27. N. Heintz, Gene expression nervous system atlas (GENSAT). *Nat. Neurosci.* **7**, 483 (2004). doi:10.1038/nn0504-483 Medline

28. N. Bodyak, B. Slotnick, Performance of mice in an automated olfactometer: Odor detection, discrimination and odor memory. *Chem. Senses* **24**, 637–645 (1999). doi:10.1093/chemse/24.6.637 Medline

29. A. Fleischmann, B. M. Shykind, D. L. Sosulski, K. M. Franks, M. E. Glinka, D. F. Mei, Y. Sun, J. Kirkland, M. Mendelsohn, M. W. Albers, R. Axel, Mice with a "monoclonal nose": Perturbations in an olfactory map impair odor discrimination. *Neuron* **60**, 1068–1081 (2008). doi:10.1016/j.neuron.2008.10.046 Medline

30. R. Hand, F. Polleux, Neurogenin2 regulates the initial axon guidance of cortical pyramidal neurons projecting medially to the corpus callosum. *Neural Dev.* **6**, 30 (2011). doi:10.1186/1749-8104-6-30 Medline

31. L. Cao, A. Dhilla, J. Mukai, R. Blazeski, C. Lodovichi, C. A. Mason, J. A. Gogos, Genetic modulation of BDNF signaling affects the outcome of axonal competition in vivo. *Curr. Biol.* **17**, 911–921 (2007). doi:10.1016/j.cub.2007.04.040 Medline

32. A. Magklara, A. Yen, B. M. Colquitt, E. J. Clowney, W. Allen, E. Markenscoff-Papadimitriou, Z. A. Evans, P. Kheradpour, G. Mountoufaris, C. Carey, G. Barnea, M. Kellis, S. Lomvardas, An epigenetic signature for monoallelic olfactory receptor expression. *Cell* **145**, 555–570 (2011). doi:10.1016/j.cell.2011.03.040 Medline

33. D. J. Rodriguez-Gil, D. L. Bartel, A. W. Jaspers, A. S. Mobley, F. Imamura, C. A. Greer, Odorant receptors regulate the final glomerular coalescence of olfactory sensory neuron axons. *Proc. Natl. Acad. Sci. U.S.A.* **112**, 5821–5826 (2015). doi:10.1073/pnas.1417955112 Medline